Bulletin of Volcanology (2017) 79: 88
https://doi.org/10.1007/s00445-017-1177-x

RESEARCH ARTICLE

Evidence for the relative depths and energies of phreatomagmatic explosions recorded in tephra rings

Alison H. Graettinger[1] · Greg A. Valentine[2]

Received: 17 April 2017 / Accepted: 15 November 2017 / Published online: 28 November 2017

Abstract Experimental work and field observations have inspired the revision of conceptual models of how maar-diatreme eruptions progress and the effects of variable energy, depth, and lateral position of explosions during an eruption sequence. This study reevaluates natural tephra ring deposits to test these new models against the depositional record. Two incised tephra rings in the Hopi Buttes Volcanic Field are revisited, and published tephra ring stratigraphic studies are compared to identify trends within tephra rings. Five major facies were recognized and interpreted as the result of different transportation and depositional processes and found to be common at these volcanoes. Tephra rings often contain evidence of repeated discrete phreatomagmatic explosions in the form of couplets of two facies: (1) massive lapilli tuffs and tuff breccias and (2) overlying thinly stratified to cross-stratified tuffs and lapilli tuffs. The occurrence of repeating layers of either facies and the occurrence of couplets are used to interpret major trends in the relative depth of phreatomagmatic explosions that contribute to these eruptions. For deposits related to near-optimal scaled depth explosions, estimates of the mass of ejected material and initial ejection velocity can be used to approximate the explosion energy. The 19 stratigraphic sections compared indicate that near-optimal scaled depth explosions are common and that the explosion locations can migrate both upward and downward during an eruption, suggesting a complex interplay between water availability and magma flux. Reverse to normal coarse-tail graded tuff breccias inferred to be the product of closely timed phreatomagmatic explosions, and deposits of magmatic gas-driven explosions, were observed interspersed with discrete explosion deposits. This study not only provides a framework for more detailed interpretations of eruption sequences from tephra rings but also highlights the gap in our understanding of syn-eruptive hydrology and variations in magma flux that enables phreatomagmatic explosions.

Keywords Tephra ring · Phreatomagmatic eruption · Explosion energy · Explosion depth · Ballistic curtain

Introduction

Tephra rings are accumulations of debris ejected from a crater by explosive eruptions typically associated with phreatomagmatic-dominated volcanic constructs like maar-diatremes. These deposits have a range of bed thicknesses, structures, grain size characteristics, and sorting (Sohn and Chough 1989; White 1991; Vazquez and Ort 2006; Valentine et al. 2015), as well as differing proportions of juvenile versus lithic components with height and distance (Valentine 2012; Chako Tchambe et al. 2015). The deposit variations, particularly coarse-grained tuff breccias or lapilli tuffs alternating with thinly stratified to cross-stratified tuffs and lapilli tuffs, have been interpreted to be a result of primary explosion processes controlled by the efficiency of phreatomagmatic fragmentation and clogging of the vent (Wohletz and Sheridan 1983; Haller and Nemeth 2006; Brand et al. 2009; van Otterloo et al. 2013; Chako Tchambe et al. 2015). The presence of deposits from Strombolian explosions, Hawaiian fallout, and lava flows—i.e., processes driven by magmatic volatiles—below, interbedded with, and capping tephra rings adds to the complexity of these eruption sequences (White 1991; Aranda-Gomez et al. 1992; Brand and Clarke 2009; Valentine and Cortés 2013; van Otterloo et al. 2013).

Recent experiments indicate that very different deposits, in terms of ejecta distribution, grain size, and bedding structure around, and away from, a crater, can be produced by a single

Editorial responsibility: J. Dufek

✉ Alison H. Graettinger
graettingera@umkc.edu

[1] Department of Geosciences, University of Missouri-Kansas City, 420 Flarsheim Hall, 5110 Rockhill Road, Kansas City, MO 64110, USA

[2] Department of Geology, University at Buffalo, 126 Cooke Hall, Buffalo, NY 14226, USA

explosion mechanism (Graettinger et al. 2015a, b), simply due to variations in depth and energy release (parameterized together as scaled depth), and the presence or absence of a crater (Goto et al. 2001; Taddeucci et al. 2013; Graettinger et al. 2015a, b; Sonder et al. 2015). These effects may partly, or completely, overprint the effects of magma flux, magma volatile content, magma viscosity, degree of fragmentation, and availability of external water on the resulting tephra ring deposits.

Tephra ring deposits record ballistic transport of debris, dilute and concentrated density currents, tephra fall, spatter, and lava flows. This work documents the presence and relative abundance of these depositional facies in incised tephra ring deposits in the Hopi Buttes Volcanic Field (HBVF) of the Navajo Nation, AZ, USA. We focus on contrasting similar tuff breccia deposits that preserve evidence of two different explosive events: discrete explosions that transport material ballistically and relatively more sustained explosion events that feed concentrated pyroclastic density currents (PDCs).

The sequences of depositional facies within tephra rings are interpreted to be a reflection of the explosions that successfully ejected material from the crater and the conditions in which those explosions occurred. For phreatomagmatic explosions, these conditions include scaled depth, or the relative depth for a given energy of an explosion within a debris filled vent, and whether the explosions were separated or closely spaced in time. The presence of magmatic explosion products record additional variations during an eruption scenario. The HBVF deposits are similar to stratigraphic descriptions published on other tephra ring sequences (Fisher and Waters 1970; Sohn and Chough 1989; Aranda-Gomez et al. 1992; Nemeth et al. 2001; Haller and Nemeth 2006; Carrasco-Núñez et al. 2007; Brand and Clarke 2009; Brand et al. 2009; Vazquez and Ort 2006; Geshi et al. 2011; Valentine 2012; Valentine and Cortés 2013; van Otterloo et al. 2013; Valentine et al. 2015). The recognition of these depositional facies in published stratigraphic sections from multiple volcanic fields enables a comparison of a wide range of tephra rings. Through the reevaluation of tephra ring sequences, it is possible to determine what is common among these sequences, and what, if any trends in eruption sequences, occurs during maar-forming eruptions.

Methods

Twelve days of field work was conducted at Teshim and Triplets tephra rings in the HBVF in 2015. Work included detailed descriptions of individual beds including bed thickness, componentry, maximum clast size, nature of contacts, clast versus matrix support, and evolution of units with distance away from the crater. Field descriptions were used to produce stratigraphic columns and fence post diagrams. New field observations were compared with existing published descriptions of the outcrops (White 1991; Newkirk 2009). Deposits were reinterpreted with perspectives from recent explosion experiments (Graettinger et al. 2015a, b). A range of initial eruption velocities for selected beds within the tephra rings were calculated based on maximum block diameters using the program Eject! (Mastin 2001). Blocks were selected from beds with evidence of ballistic emplacement and extensive descriptions from the field to constrain block position relative to the vent and bed thickness with distance from the vent. The volume of selected beds containing these clasts was then estimated using a simplified geometry using the thickness of those beds in proximal and distal locations assuming a symmetrical distribution. A range of reasonable deposit densities (1900–2500 kg/m^3) was then applied to these volumes to estimate deposit mass.

Several tephra rings described in previous publications were selected for reevaluation including Tito Maar (Haller and Nemeth 2006) (Argentina); Mt. Gambier (Van otterloo et al. 2013; Van Otterloo and Cas 2016) (Australia); Tihany Maars (Nemeth et al. 2001) (Hungary); Straciacappa (Valentine et al. 2015) (Italy); Suona Crater (Geshi et al. 2011) (Japan); Atexcac (Carrasco-Núñez et al. 2007; López-Rojas and Carrasco-Núñez 2015), La Brena-El Jaguey (Aranda-Gomez et al. 1992), and Tepexitl (Austin-Erickson et al. 2011) (Mexico); Suwolbong tuff ring (Sohn and Chough 1989) (South Korea); and Easy Chair (Valentine and Cortés 2013), Fort Rock (Brand and Clarke 2009), Haskie Maar (Vazquez and Ort 2006), Narbona Pass (Brand et al. 2009), Salt Lake Craters (Fisher and Waters 1970), Ubehebe Craters (Fisher and Waters 1970; Fierstein and Hildreth 2017), and Zuni Salt Lake Maar (Fisher and Waters 1970) (USA). Tephra rings selected had stratigraphic columns, field photos, or descriptions with sufficient detail to be compared with facies descriptions produced during field work at HBVF. Comparison between field observations and published studies was used to determine if a previously studied tephra ring contained facies observed at HBVF. When possible, the relative abundance of those facies was noted as well as any facies associations. The examples selected for reevaluation are not exhaustive of available tephra ring studies but were determined to represent a range of magma compositions, ages, tectonic settings, and geographic locations.

Geologic setting of the Hopi Buttes Volcanic Field

The HBVF is a 7-Ma, mafic monogenetic field with partially preserved craters and tephra rings in the north and diatremes exhumed up to 300 m below the eruptive surface to the south (White 1991; Lefebvre et al. 2013; Muirhead et al. 2016). In the northern part of the field, several tephra rings formed by phreatomagmatic eruptions involving alkaline mafic magmas are preserved beneath capping lava flows (Fig. 1). Teshim Butte (35° 32′ 17″ N, 110° 07′ 05″ W) preserves ejecta in

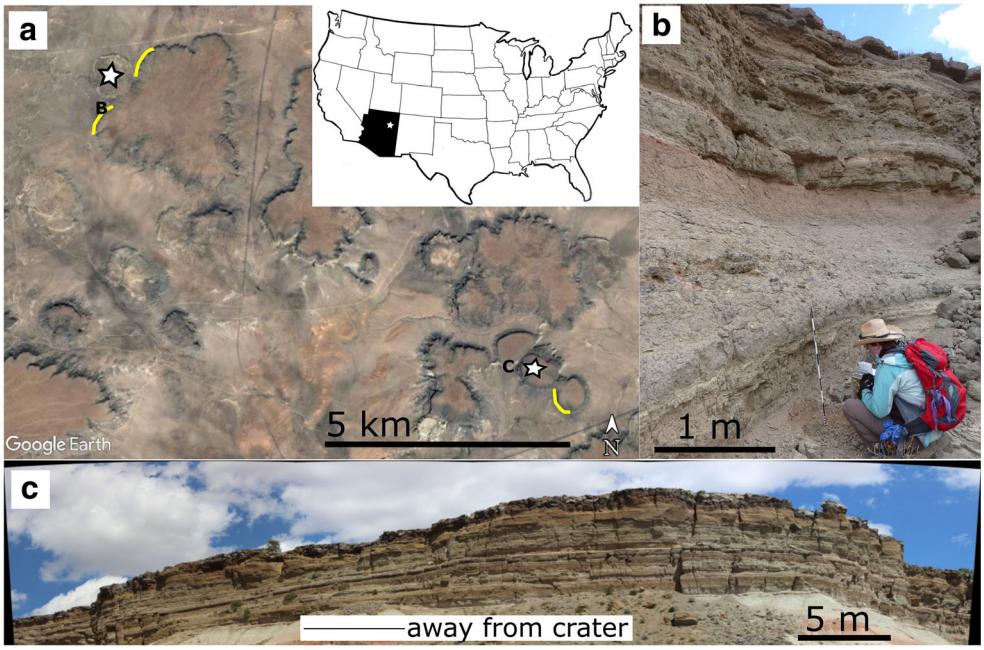

Fig. 1 Location of Teshim and Triplets tephra rings in the Hopi Buttes Volcanic Field (Navajo Nation, AZ, USA). **a** Aerial view of the northern part of the HBVF with stars on Teshim (western) and Triplets (eastern) locations, white stars are located in craters and yellow lines highlight outcrops discussed in detail in the text. **b** Example of stratigraphy exposed in the Teshim tephra ring. The layered deposits show variability in thickness, componentry, and grain size. Location indicated on **a**. **c** Image of the northern portion of the Triplets tephra ring where variations in grain size and componentry result in visibly traceable beds over tens of meters. Location indicated on **a**

two directions along the eastern margin of Teshim Crater, and isolated outcrops are preserved to the southwest (White 1991). Previous work on the crater fill and tephra ring established a basic stratigraphy including a range of deposits attributed to PDCs, as well as monomictic, well-sorted deposits interpreted as fallout (White 1991). Similarly, the Triplets crater (35° 28′ 58″ N, 110° 01′ 14″ W) has two radial outcrops of ejecta that were described by Newkirk (2009) as containing bedded and cross-bedded lapilli tuffs interpreted to be the products of dilute PDCs, massive poorly sorted tuff breccias interpreted as concentrated PDC deposits, and minor scoria and spatter deposits. The maar-diatremes cut through the same stratigraphy of 30–100 m of unconsolidated silty sediment and weak silty sandstones of the Mio-Pliocene Bidahochi Formation, underlain by Triassic sandstones and Chinle shales and muds (White 1991). We recognized previously described units at both sites and identified additional facies in deposits previously called 'surge containing sequences' that contained cross-bedded tuffs with interbedded massive, block-rich layers. These form couplets of alternating tuff breccia or lapilli tuff with stratified to cross-bedded tuffs to lapilli tuffs that make up a significant portion of the stratigraphic sequence at both locations.

Facies

Five facies, as defined by common structure, componentry, grain size distribution, and lateral evolution, were common at both Teshim (Fig. 2) and Triplets (Fig. 3) and resemble deposits described at other tephra rings. The Triplets sequence has an additional facies of a capping welded agglomerate. These facies are described in the proximal (< 100 m from the crater rim) to distal reaches (up to 1 km) to enable interpretation of transport and deposition processes (Table 1). The Teshim maar sequence is ~ 15 m thick proximal to the crater, but thins to 6 m thick within 500 m and is not preserved or recognized beyond 1 km (White 1991). The Triplets deposit is ~ 19 m thick proximally and thins to about 1 m thick by 1 km distance (Newkirk 2009). Both of these maars are hosted by the same sequence of country rock and were produced by similar alkaline mafic magmas and therefore have very similar componentry. The basaltic (loosely referring to the alkaline mafic materials) components of the two sequences show minor differences, where at Teshim the basaltic components are universally dense (vesicularity < 30%), while at Triplets basaltic clasts can be more vesicular (40–50%) and occasionally show red iron oxide coloration. The basaltic clasts at the two sites likely include both juvenile and recycled clasts (Graettinger et al. 2016) and are only identified as juvenile or lithic clasts when additional information allows such distinctions.

Massive tuff breccia and lapilli tuff (TBm)

Poorly sorted, variably matrix- to clast-supported, beds of massive tuff breccia (Fig. 4) have a matrix composed of fine to coarse ash and lapilli with blocks up to 60 cm in diameter (Table 1). Blocks contribute up to 80% of deposit volume. Proximal bedding is crudely developed and is defined by concentrations of different block types and grain size variations (Fig. 5). These poorly defined beds are 10–50 cm thick and occur in sets between 2 and 8 m thick. Bedding is locally difficult to delineate because blocks are occasionally larger than the thickness of a bed, and the bases of layers frequently

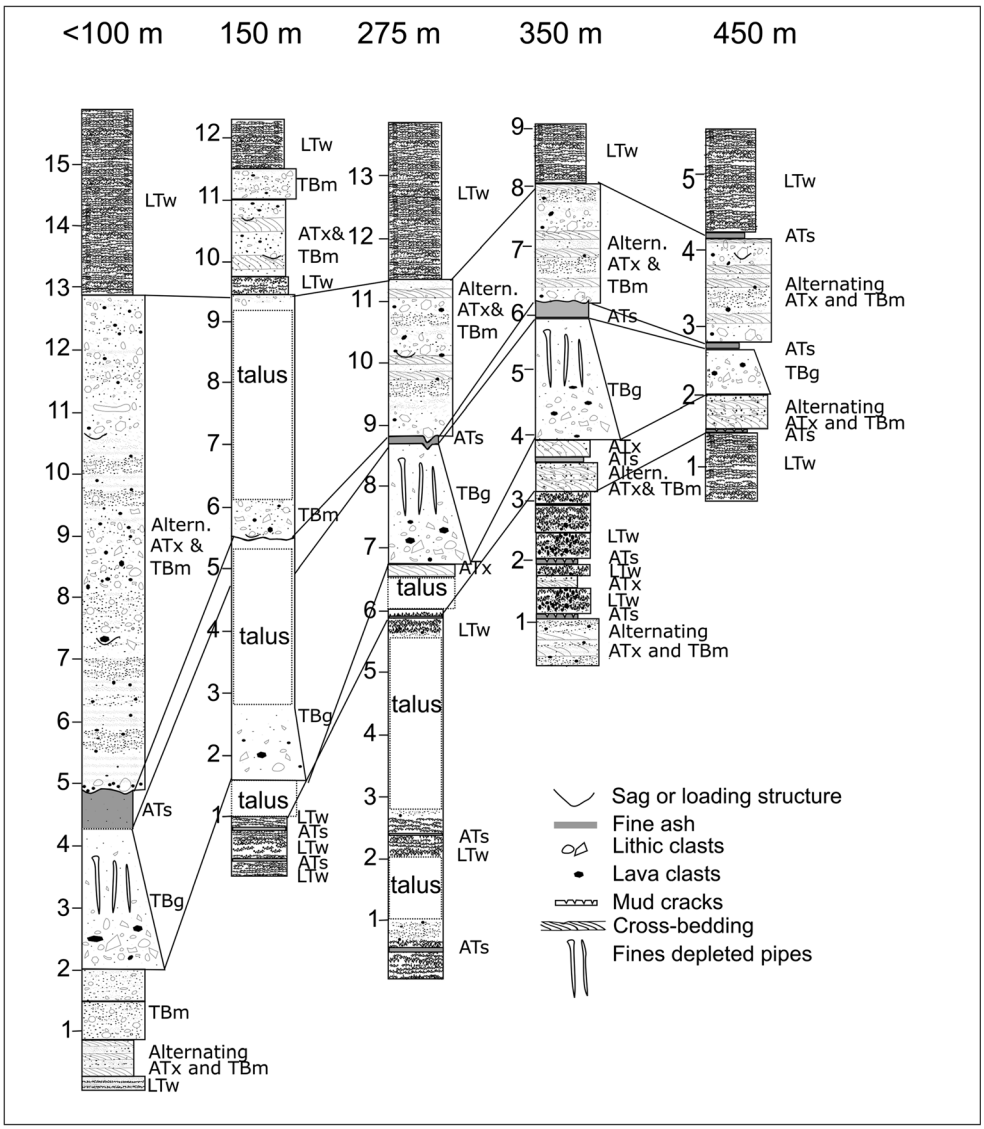

Fig. 2 Stratigraphy of the southeastern outcrop of Teshim Butte in Hopi Buttes Volcanic Field. Site marked on Fig. 1a. Major units correlate with descriptions in White (1991)

contain loading structures and bomb sags that disrupt contacts (Fig. 6). Bedding becomes more distinct with increasing distance from the crater, and beds of TBm are separated by ash and lapilli-dominated layers (mainly cross-bedded ash and lapilli tuff (ATx) and well-sorted ash (ATs)). The size and abundance of large blocks decreases with distance from the crater. Typically, beds mantle topography (tens of centimeter variations) but have undulatory contacts (centimeter undulations). Although the number of beds within a bed set is difficult to count precisely, the number of beds in distal outcrops decreases and the beds thin. By 400 m distance from the crater, bed sets containing TBm are 2 m or less in thickness, with beds well separated by tuffs. This results in a wedge shape for TBm bed sets (Fig. 2).

Massive tuff breccias contain a range of block types including basaltic (60–80%), sedimentary lithic (20–40%), and composite clasts (< 1%). Basaltic clasts have angular to subrounded shapes that are mostly equant with both ropey surface textures and fractured faces. Lithic clasts include clasts of country rock from units beneath the current level of erosion and clasts of bedded tuff (see White 1991). Silty lithic blocks from the shallow Bidahochi Formation have distinctive fluidal structures and sandstone and tuff blocks are subrounded to subangular. The relative abundance of the two lithic types varies between layers and with distance. Some lithic blocks are fractured and preserved as jigsaw fit clusters or short trains with variable amounts of matrix between grains (Fig. 6b). Lithic clast clusters may contain individual clasts up to 50 cm in diameter and clusters sometimes reach up to 2 m long. These clusters and elongate clasts are typically oriented parallel to bedding and aligned radially away from the crater (Fig. 7). Blocks of bedded lapilli tuff are rare (< 1%) and can be up to 20 cm. Composite clasts reach 10 cm in size and have a sedimentary lithic core surrounded by basalt with an equant shape. The relative abundance of clast types varies between individual layers and with distance. Locally, beds may be

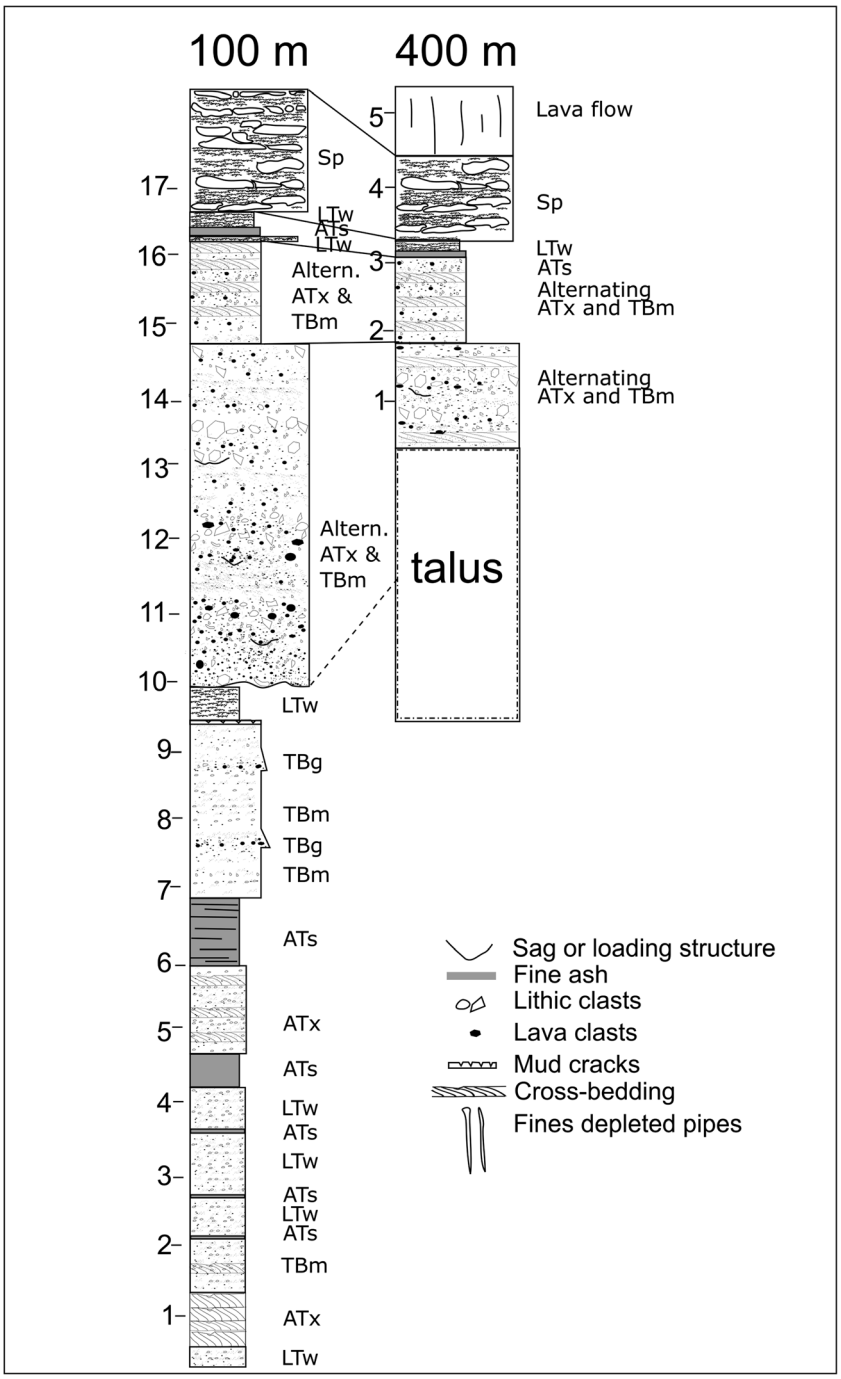

Fig. 3 Stratigraphy of southeastern outcrop at Triplets in the Hopi Buttes Volcanic Field, Navajo Nation, AZ. Location marked on Fig. 1a

dominated by a single clast type and are traceable for 10–100 m laterally. While lithic clasts only make up 20–40% of the blocks, they make up a large component of the finer grain fractions in the form of disaggregated particles from unconsolidated silts, fine sands, and weak siltstones of the Bidahochi Formation (White 1991).

Interpretation The TBm deposits are dominated by their poor sorting, lack of internal structure, abundant large lithic clasts with fluidal to jigsaw shapes, and loading structures along their base. The bedding surfaces are not planar and the contacts are not perfectly parallel. While crude bedding is visible in proximal locations, individual beds are nearly structureless from proximal to distal locations. Beds mostly mantle underlying surfaces and do not preferentially fill in minor topographic lows. This suggests that this deposit is not produced by a density current, even though it is poorly sorted, but it may have experienced minor sliding or saltation before deposition. Loading structures and bomb sags along the basal contact reflect very rapid sedimentation,

Table 1 Lithofacies descriptions and interpretation of tephra ring deposits

Facies	Description	Interpretation	Previous interpretation
TBm	Poorly sorted massive tuff breccia. Matrix- to clast-supported. Basal contact has loading structures and the top is undulatory. Beds mantle topographic variations. Heterolithic componentry. Individual beds are 10–50 cm thick. Beds of TBm become more discrete and frequently occur alternating with ATx distally. Blocks make up to 80% of deposit volume and reach 60 cm. Basalt blocks are subrounded to angular, while siltstone and sandstone blocks are subrounded to fluidal to jigsaw shape.	Ballistic curtain deposits formed by discrete explosions through a debris-filled vent. A poorly sorted mixture of clasts travels along a ballistic trajectory and may experience local sliding or bouncing (saltation) upon impact. Frequently trailed by dilute density currents creating couplets in depositional sequence representing a single explosion event.	Dense pyroclastic density current with isolated ballistic impacts. In many cases not distinguished as a separate lithofacies
ATx	Moderately sorted cross-bedded lapilli tuff that is matrix-supported and fills in topographic lows. Short, centimeter-long chains of lapilli help highlight 0.5–2 cm laminations. The upper contact is typically flat. Multiple truncations and internal erosional structures, including dune forms, are typical. May be deformed by overlying unit, including bomb sags. Subangular lapilli and coarse ash of a range of component types. Pink to white color suggesting abundant fine-grained lithics. Layers are 1–50 cm thick and can be stacked or interbedded with TBm.	Dilute pyroclastic density currents. Currents can be produced by the collapse of a dilute eruption column, the lateral expulsion of fines from the collapse of poorly sorted debris into a crater, or from trailing fines following a ballistic curtain.	Dilute pyroclastic density currents formed by the collapse of dilute eruption columns
TBg	Poorly sorted matrix-supported tuff breccia with reverse to normal coarse-tail grading of blocks. Highest concentration of outsized clasts is just above the basal contact. Beds are 10–300 cm thick. Blocks are subrounded to subangular heterolithic clasts < 30 cm that make up 40% of the deposit. Basalt blocks are poorly vesiculated (10–40%) with subrounded to irregular shapes. Proximally, the lower contact may be erosional and subvertical fines-depleted pipes are common in the upper half of deposit. Locally fills in topographic lows.	Concentrated pyroclastic density current formed by the collapse of an eruption column produced by a sustained eruption through a debris-filled vent. Fines-depleted pipes are interpreted as gas escape structures.	Same
LTw	Clast-supported, well-sorted, medium to coarse lapilli tuff with discrete subplanar beds up to 50 cm. Contains basaltic clasts and isolated crystals with rare sedimentary lithic clasts. All clasts are angular to subrounded with low vesicularity (10–40%). LTw beds may be separated by centimeter-thick fine ash (ATs) layers.	Pyroclastic fall deposit of recycled clasts. Associated with the formation of the maar suggested from the repetition of these layers early and late in the sequence and the presence of rare lithic clasts.	Pyroclastic fall deposits associated with the formation of the maar
ATs	Well-sorted fine ash with rare outsized lapilli. Basal contact can be gradational or sharp. Pink to white ATs beds contains mostly lithic components. Beds can be 1 to 50 cm thick and are associated with TBg, ATx, and Tm beds. Brown ATs beds occur in between LTw and are 1–3 cm thick.	White and pink ATs layers are accessory fall (lithic-rich). Delayed deposition of suspended fines by explosions through a debris-filled vent. Brown ATs layers are likely related with LTw producing events.	Not always distinguished as a separate lithofacies, but when recognized the interpretation was the same.
Sp	At Triplets, the upper LTw transitions locally into spatter and agglutinate that reaches 2 m in thickness. Bombs are 30–70 cm in diameter with fluidal textures and occur in a matrix of 1–3 cm clasts that are variably matrix to clast-supported. Clasts are locally welded. Transitions upward into a lava flow with faint relict clasts visible.	Agglomerate and clastogenic lava	Same

and large jigsaw clasts argue against prolonged flow. These features suggests a ballistic emplacement of a mass of material that is a mixture of grain sizes from a discrete explosion, in other words a granular dispersion that follows a ballistic path rather than only individual clasts, called a ballistic curtain by Graettinger et al. (2015a). These

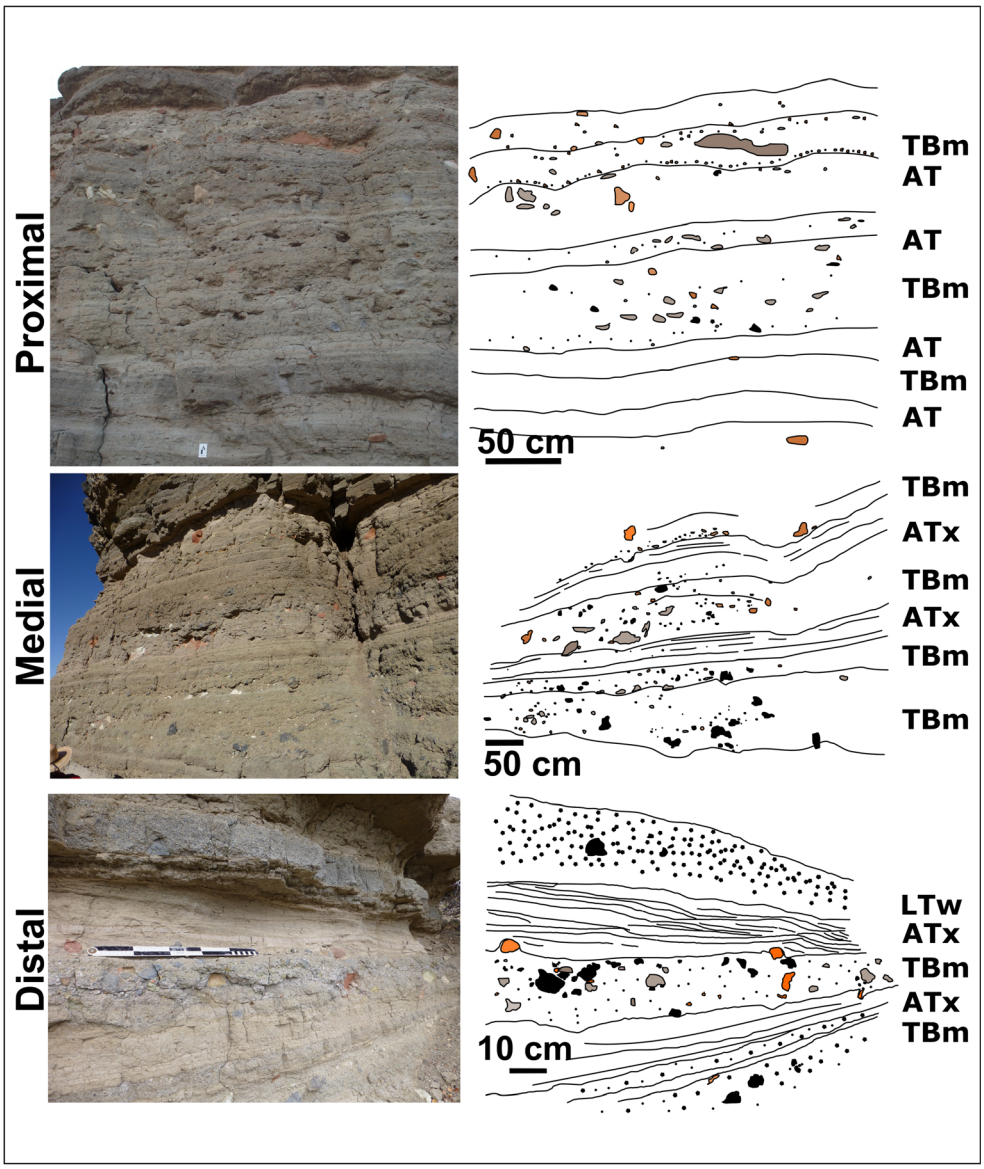

Fig. 4 Massive tuff breccia (TBm) deposits from Teshim maar interpreted to be the product of ballistic curtains formed by discrete explosions through a debris-filled vent. Well-sorted lapilli tuff (LTw) in lower image is interpreted as a pyroclastic fall unit. Lines are used to indicate bedding and major clasts are outlined. Colors reflect different clast types: orange and gray are lithics, black is basaltic. Proximal image 35.534022° N, 110.117524° W; medial image 35.541845° N, 110.110632° W; distal image 35.531626° N, 110.119804° W

deposits match well with deposits formed by ballistic curtains produced by subsurface explosion experiments (Graettinger et al. 2015a). This similarity includes the very thick proximal deposits, more consistent medial blanketing deposits, and thin to isolated clasts in distal deposits. Radial orientation and alignment of bombs and block clusters away from the crater observed in Teshim and Triplets are similar to experimental deposit rays associated with

Fig. 5 Proximal couplet of TBm and finer grained ash-rich units that develop into ATx with distance away from the source (100 m from crater rim Triplets). Lines are used to indicate bedding and major clasts are outlined. Colors reflect different clast types: orange and gray are lithics, black is basaltic. Image location: 35.479838° N, 110.015998° W

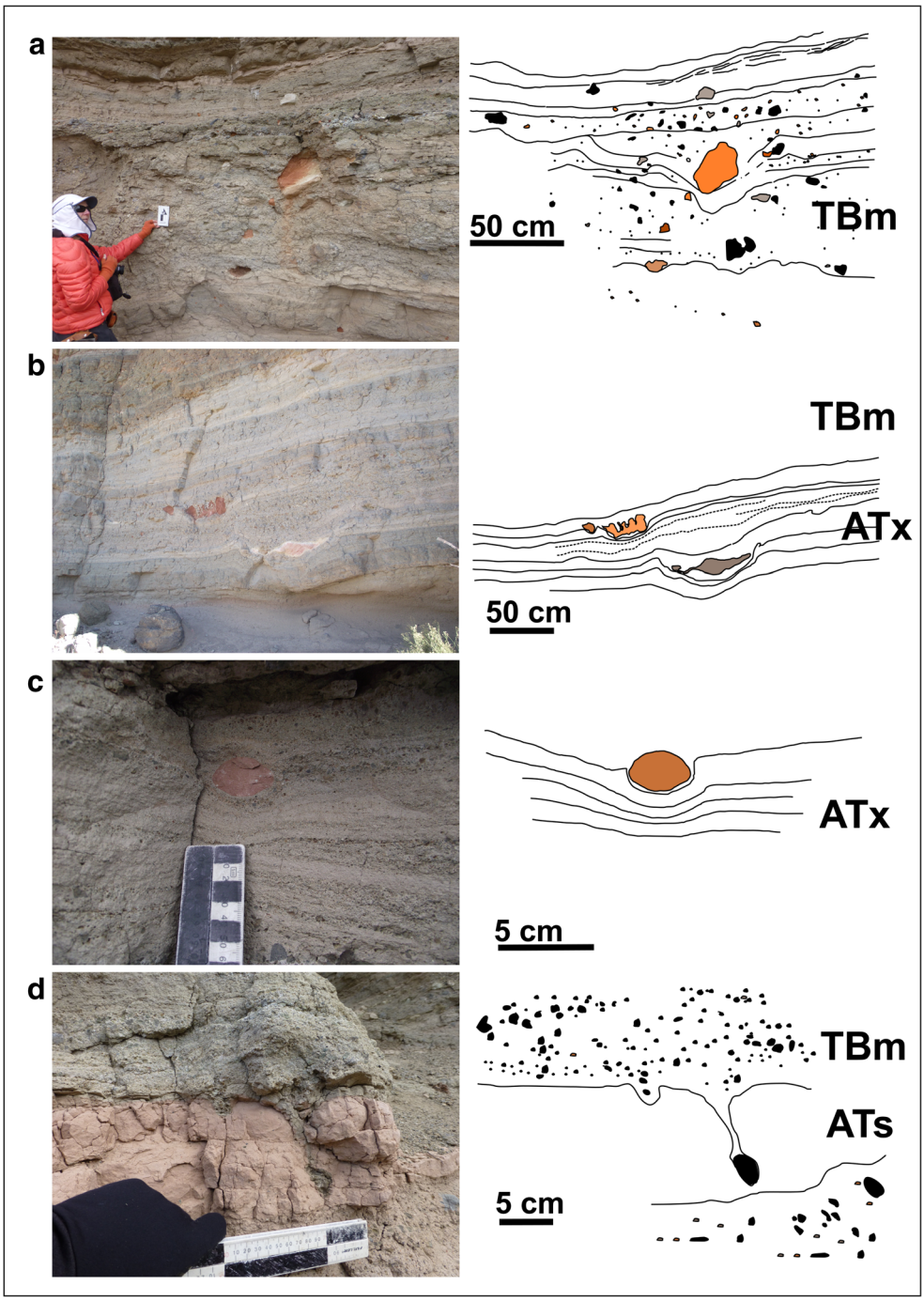

Fig. 6 Stratigraphic contacts disrupted by the impact of ballistically transported material including: **a** masses of poorly sorted debris impacting into layered TBm and ATx; **b–d** individual clasts and jigsaw clasts in bed sets of TBm and ATx or ATs (various distances Teshim). Lines are used to indicate bedding and major clasts are outlined. Colors reflect different clast types: orange and gray are lithics, black is basalt. Image locations: **a** 35.531826° N, 110.119561° W; **b** 35.541113° N, 110.111310° W; **c** 35.52877° N, 110.119207° W; **d** 35.531626° N, 110.119804° W

explosion jet instabilities in shallow explosions (Graettinger et al. 2015b). Experimentally produced ballistic curtain deposits also exhibited radial and lateral variations in componentry as a result of the available material above the explosion site (Graettinger et al. 2015b), similar to componentry variations observed within and between TBm units at Teshim. The proximally thick to medial blanket of poorly sorted tuff breccia with depositional lower contacts reflects a distinct depositional mechanism from concentrated flows of debris.

Cross-bedded ash and lapilli tuff (ATx)

Ash and lapilli tuff with rare blocks comprise 10–50 cm thick beds with planar, dune form, and truncated cross-beds, which themselves are formed by laminae to very thin layers on the order of 0.5–2 cm thick (Fig. 8; Table 1). Beds can be traced laterally for hundreds of meters. ATx may thicken in topographic lows and may occur with other ATx layers, or immediately above or below TBm layers. Isolated blocks up to 4 cm in diameter with subangular to subrounded shapes are present

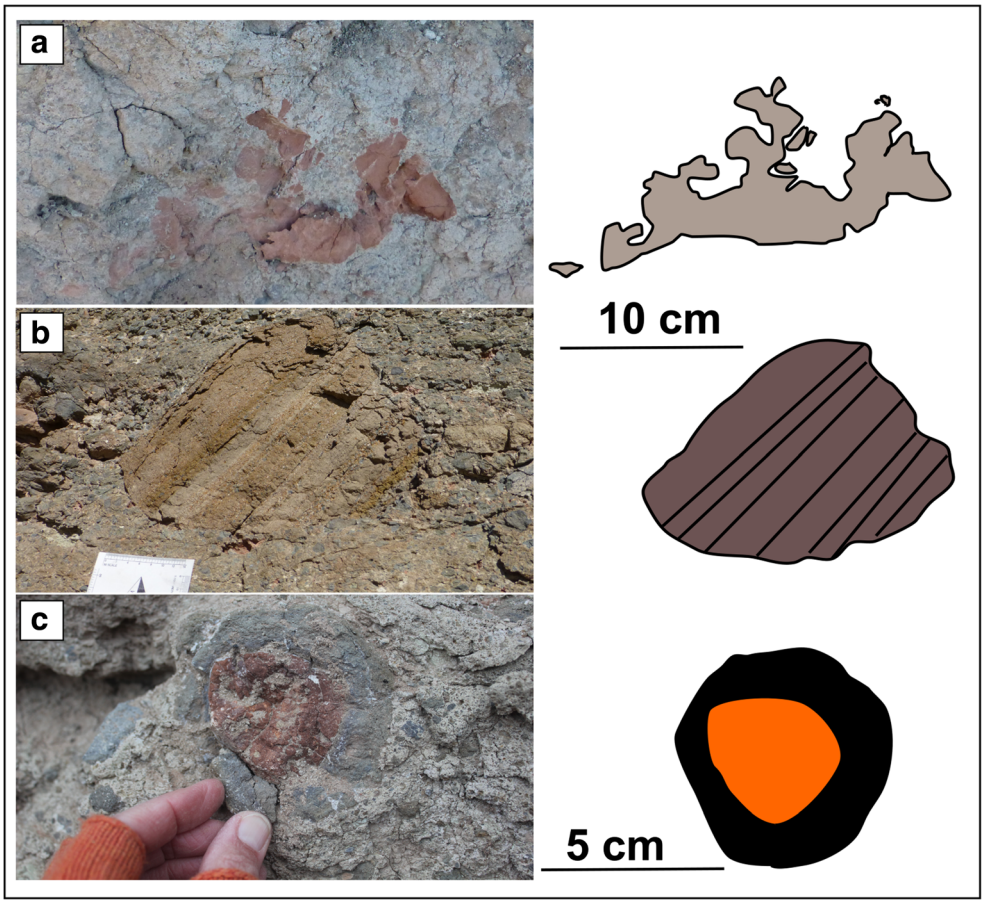

Fig. 7 Unique clast types found within massive tuff breccia. **a** Jigsaw clast of Bidahochi mudstone; these clasts are only found in TBm. **b** Clasts of bedded tuff. **c** Composite clasts composed of sedimentary lithic surrounded by basalt

and visibly make up about 1% of individual units. Sags frequently occur along the tops of ATx layers when they are overlain by TBm, and internal block sags are common (Fig. 6c). The color of ATx varies from white to pink reflecting the presence of particles sourced from sedimentary lithic materials (i.e., Bidahochi silt; White 1991). Lapilli and block-sized components are basalt and sandstone clasts. Cross-bedding and dune structures are commonly described in other tephra ring stratigraphic descriptions (Fisher and Waters 1970; Sohn and Chough 1989).

Interpretation The dominance of dune-form structures and the more limited grain size distribution of these deposits suggest lateral transport by dilute density currents. These currents are frequently called base surges and have been observed from eruptions in emergent marine environments (Moore 1967) and through crater lakes (Waters and Fisher 1971). Such dilute density currents can be formed through the collapse or fountaining of a dilute eruption column (Fisher and Schmincke 1984). Experiments have shown that dilute density currents can be produced from the collapse of vertically focused, dense columns of material into a crater, which causes lateral expulsion of gas and fines, and do not require collapse of already-dilute eruption columns (Graettinger et al. 2015a). The rapid sedimentation from ballistic curtains would further expel fines that continue to travel in the direction of transportation and form dilute density currents; in experiments, ballistic curtains were often trailed by a fine-grained, dilute flow (Graettinger et al. 2015a). Detailed descriptions and discussions of various fine-grained deposits produced by dilute density currents by Sohn and Chough (1989) highlight the lateral evolution of dilute density current deposits and illustrate that dilute density currents do not have to include dune forms or cross-bedding. Individual ATx beds contain abundant signatures related to flow behavior, but the relationship between underlying and overlying facies is critical to interpreting their generation.

Coarse-tail graded tuff breccia (TBg)

TBg is a poorly sorted, matrix-supported tuff breccia with coarse-tail grading of blocks in a lapilli and coarse ash matrix and was described in detail by White (1991) at Teshim (Fig. 9; Table 1). TBg deposits are up to 3 m thick at Teshim with abundant blocks up to 30 cm in diameter. At Triplets, these deposits are thinner, 0.1–0.5 m, and contain large lapilli and small blocks. Large lapilli and blocks in TBg deposits are heterolithic and subrounded to subangular.

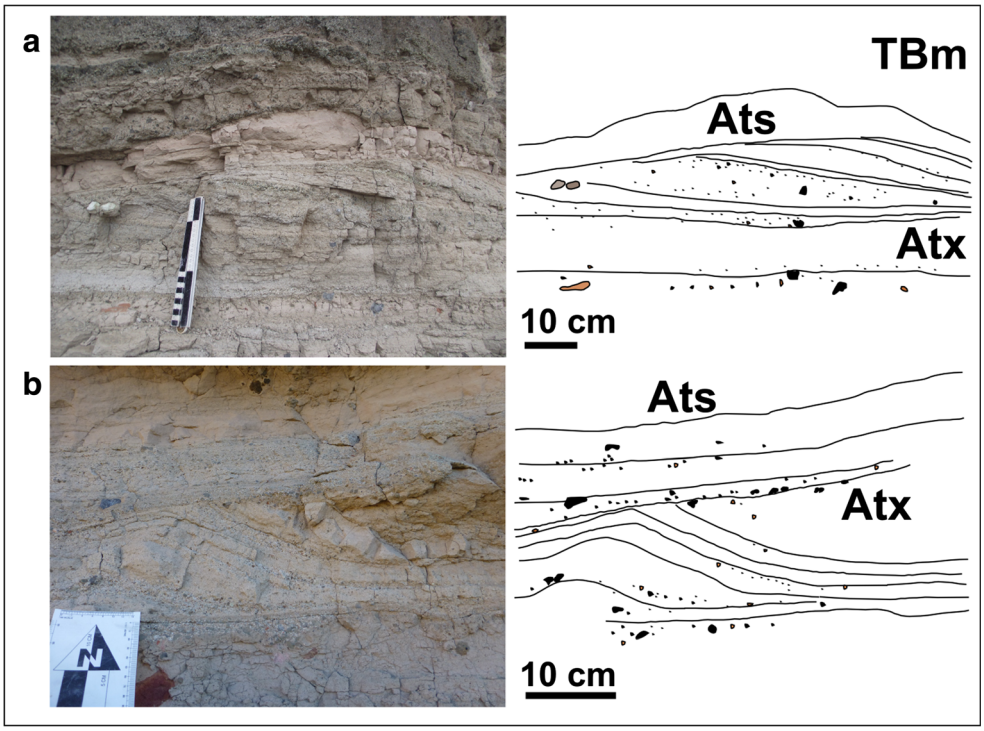

Fig. 8 Cross-bedded ash tuff (ATx) interpreted to form from dilute density currents. Cross-bedding and dune forms occur at variable scales (**a**, **b**). Well-sorted ash tuff (ATs) mantles topography and occurs between ATx and TBm, above TBg (see figure) or in between LTw units. Lines are used to indicate bedding and major clasts are outlined. Colors reflect different clast types: orange and gray are lithics, black is basalt. Image location: 35.531626° N, 110.119804° W

The largest concentration of blocks occurs a few centimeters above the base of the deposit, and the size and concentration of blocks then decreases upward producing reverse to normal coarse-tail grading. The largest blocks are typically basalt (60–90%), with sandstone lithics (10–30%) and rare siltstone lithics. The matrix is white to pinkish in color, being composed of predominantly disaggregated material of the sedimentary host (Bidahochi silt), with basalt, siltstone, and sandstone lapilli. At both Teshim and Triplets, TBg grades proximally into a massive fine pink to white tuff (ATs). Distally, these become two separate units with a sharp contact. The number and proportion of different clast types remains relatively constant with distance from the crater. The basal contact of the TBg truncates underlying units. Proximal TBg deposits commonly contain vertical to subvertical fines-depleted pipes in the upper half of the deposit and a locally erosive basal contact. Distally, the TBg can fill in topographic lows. The top of the unit remains horizontal with distance. At Teshim, the thickest TBg

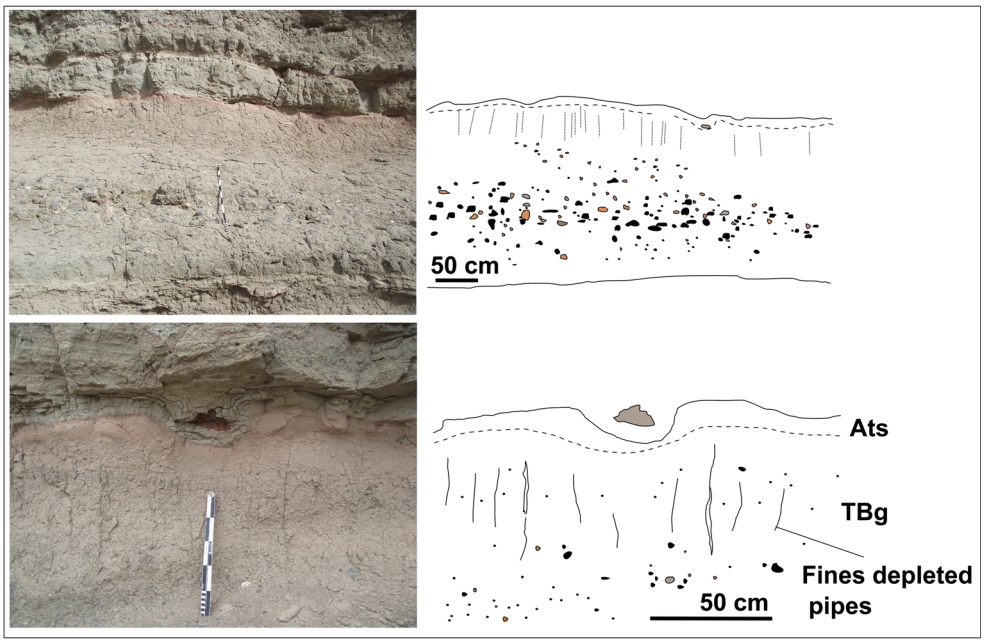

Fig. 9 Normal graded tuff breccia (TBg) interpreted to be produced by dense pyroclastic density currents from sustained eruption episodes. Lines are used to indicate bedding and major clasts are outlined. Colors reflect different clast types: orange and gray are lithics, black is basalt. Image location: 35.52877° N, 110.119207° W

unit grades vertically into a pink fine ash unit proximally, but with distance they become two discrete units.

Interpretation The combination of matrix support, normal and reverse-to-normal coarse-tail grading, proximal erosion of lower contacts, and distal topographic filling suggests lateral transport of a concentrated PDC or a dilute current undergoing very rapid sedimentation with lateral motion of a concentrated, aggrading basal zone. Fines-depleted subvertical pipes in the upper portion of the deposit are interpreted as gas escape structures, indicative of high pore pressure at initial deposition of the unit, also consistent with the above emplacement processes. White (1991) described a very prominent example of TBg at Teshim and interpreted it as the product of a concentrated PDC. We observed a few additional thinner examples of this facies in the Triplets sequence (Newkirk 2009). Concentrated PDCs or aggradation from a rapidly sedimenting, more dilute PDCs require a more prolonged supply of gas and debris compared to ballistic curtain mechanism that results from relatively discrete explosion events. The concentrated PDC could be produced by the collapse of a relatively more sustained eruption column (lasting tens of seconds to a minute) produced by closely spaced in time phreatomagmatic explosions. The componentry, in particular the abundance of fine-grained lithic material, reflects the transport of mixed debris dominated by crater fill produced by previous explosions, rather than a magmatic explosion.

Well-sorted lapilli tuff (LTw)

LTw is a clast-supported, relatively well-sorted lapilli tuff that occurs in thin beds up to 1–5 cm and forms bed sets up to 50 cm thick (Fig. 4; Table 1). Both the beds and bed sets have planar parallel bedding and do not change significantly in grain size and remain on the order of tens of centimeters thick within the study area. The exposure of LTw deposits is frequently limited in stratigraphic position to the base of the sequences, being covered by talus, or the top of the sequences where erosion has removed some layers. This facies is almost wholly composed of variably vesicular (10–40%) subangular basalt lapilli between 0.3 and 1 cm in diameter with free crystals of pyroxene and lesser plagioclase or biotite. Rare sedimentary lithic clasts contribute up to 1–3% of the deposit volume and may be the same size as basaltic lapilli or up to 5 cm in diameter. The lapilli tuff has subtle subhorizontal stratification defined by slight variations in grain size between 0.3 and 1 cm. Rarely, a fine-grained variably palagonatized ash matrix is present between clasts, but in most places, the deposits have a framework structure. Grain surfaces are frequently covered by a white-, green-, or yellow-colored mineral coating. Individual bed sets may have one or two thin (0.5–1 cm thick) horizontal interbeds of fine ash (ATs).

Interpretation The well-sorted nature and relatively homogeneous componentry of LTw implies that it was produced by fallout from an eruption cloud. The predominance of basaltic particles including free crystals indicates that this deposit was formed by explosive magmatic activity, despite the lower vesicularity of lapilli (White and Valentine 2016). The subangular to subrounded clast shapes may be reflective of recycling or reworking of the clasts. However, the absence of a matrix suggests the rounding of clasts either occurred in the vent or was the result of local grain flows. The low slope angle of the deposits and preservation of ATs between LTw beds implies that abrasion took place prior to deposition and was related to vent processes.

Well-sorted ash (ATs)

Planar bedded well-sorted fine ash (ATs) is interbedded with other depositional units specifically between ATx and TBm, above TBg and within LTw (Figs. 8 and 9; Table 1). The color of the deposit varies from brown to white to pink. Rare outsized lapilli (0.5–1 cm in diameter) make up < 1% of the deposit. The beds are locally disrupted by bomb or block sags, loading structures, channels filled by ATx, and localized faulting (Fig. 6d).

Interpretation The pink and white coloration of many ATs deposits share similarities with the near surface stratigraphic Bidahochi Formation, which contains abundant unconsolidated pink and white silt (White 1991). We therefore interpret these ash deposits as settled from a plume or density current-generated cloud of lithic ash (e.g., Nemeth et al. 2012). The association of these deposits with other coarse-grained lithic-rich facies such as TBg and TBm supports this interpretation. Conversely, ATs deposits interbedded with LTw deposits are typically brown in color and are more likely the result of settling from the same or similar eruption columns related to the formation of LTw and could contain juvenile ash, or fines produced through recycling in the vent. As LTw is made up of recycled clasts, this supports a lithic origin of the interbedded ash.

Locally welded agglomerate (Sp)

At the Triplets location, LTw grades upward into larger fluidal vesicular juvenile clasts that are locally welded (Fig. 10; Table 1). These welded basaltic clasts transition vertically and laterally into a lava flow that contains relict clast textures within the lowermost 50 cm of the flow. Bombs are 30–70 cm in diameter and aligned with the bedding. The welded unit has a local matrix of 1–3 cm sized scoria with moderate to low (< 50%) vesicularites.

Interpretation The fluidal clast shapes, local welding, and upward transition into a clastogenic lava flow indicate that

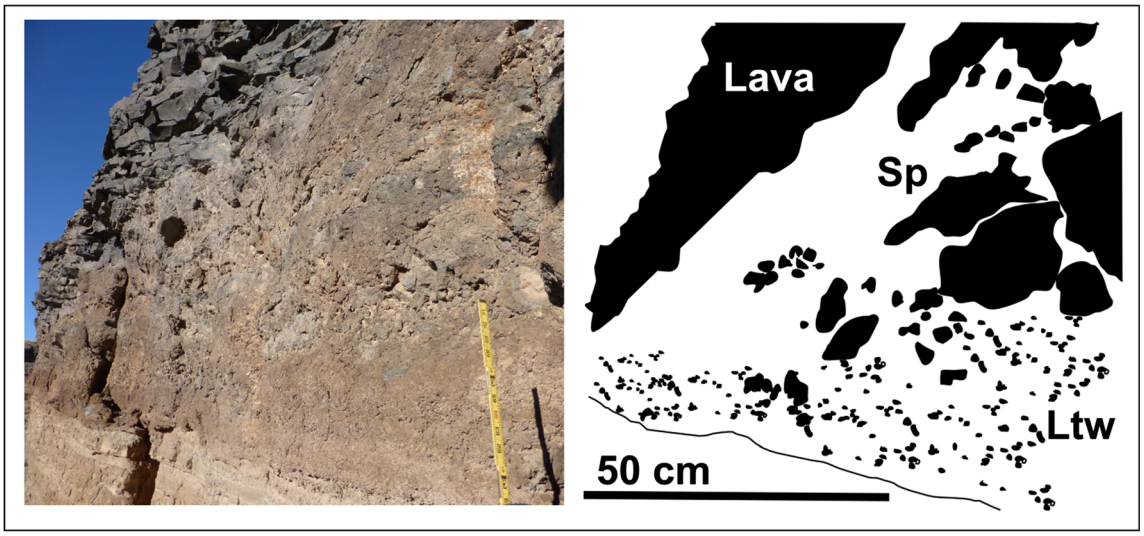

Fig. 10 Photo and sketch of Triplets tephra ring where it is capped by LTw that transitions upward into agglomerate and ultimately a clastogenic lava flow. Image location: 35.478596° N, 110.015812° W

the end of this sequence was dominated by volatile-driven fragmentation of the magma, likely in the form of fire fountaining, where clasts accumulated rapidly while still hot and deformable. This resulted in local agglutinate that transitions vertically and laterally to a lava flow that extended beyond the ballistic reach of the Strombolian activity. The resulting agglutinate and lava flow cap the sequence and preserve the vertical outcrops of the tephra ring (Fig. 10).

Facies associations

Both the Teshim and Triplets tephra rings contain the first five facies (Sp only occurs at Triplets) in variable abundances, thicknesses, and order. In addition to the similarity of facies, the two tephra rings also had similar facies associations. Coarse-tail graded tuff breccia (TBg) units are typically gradationally covered by white to pink well-sorted fine ash (ATs) proximal to the crater (< 400 m), but both facies thin and the contact between them becomes sharper with distance (Figs. 2, 3, and 9). This suggests that ATs units capping TBg units are coeval with the PDC that produced the underlying TBg; fine ash is lofted by the flow and eventually settles after the flow ends. Thin ATs units also occur with other facies such as cross-bedded tuff (ATx; Figs. 2, 3, and 8) where unit contacts are sharp, except when disrupted by bomb or block sags (Fig. 6d). Here the ATs unit is interpreted as the result of delayed settling of suspended ash genetically related to the dilute density current that formed the ATx deposit.

Massive tuff breccia (TBm) and cross-bedded tuff (ATx) typically occur in sequences of couplets of TBm overlain by ATx. Individual couplets become more obvious with increasing distance from the crater as contacts become more distinct (Figs. 4 and 5). Sequences containing TBm and ATx couplets may include multiple overlapping TBm units, which can be difficult to distinguish except in cases of distinct clast types within a given massive tuff breccia. Similarly, repeated beds of ATx were observed between, below, and above couplets or other facies. This makes precise counting of the number of beds difficult, though minimum estimates are possible. The tephra ring sequence at Triplets contains at least ten couplets within a single 5–8-m-thick bed set, while at least seven were observed at Teshim in a similar thickness bed set. Mixed within these bed sets are also isolated well-sorted fine ash layers (ATs) found above cross-bedded tuffs (ATx). These ATs beds have heavily modified upper contacts from loading structures from overlying TBm (Fig. 6).

The occurrence of massive tuff breccia with overlying cross-bedded tuff and occasional fine ash beds corresponds to the order of events observed in explosion experiments by Graettinger et al. (2015a), where an explosion lofted poorly sorted debris upward before expanding outward and downward as a ballistic curtain, emplacing a blanket of poorly sorted debris that was very thick proximally, formed a sheet-like blanket medially, and diffuse isolated clasts distally. This deposit was then covered by a related dilute, finer-grained density current that trailed the coarser more poorly sorted ballistic curtain (Graettinger et al. 2015a). The dilute density current was then followed by delayed setting of fine particles. Each couplet, and ash cap if present, therefore, can be inferred to represent the deposits from a single explosion. These couplets have many similarities with deposits associated with individual lateral blasts resulting from rapid unloading of pressurized domes/cryptodomes or hydrothermal systems (e.g., Belousov et al. 2007; Breard et al. 2015).

The occurrence of multiple couplets reflects a repeating process of individual discrete explosions that transport material out of a crater through two distinct, but related,

mechanisms. This contrasts with previous work that interpreted coarse and fine beds as separate events reflecting variations in either efficiency, explosion location, or abundance of water (Wohletz and Sheridan 1983; Haller and Nemeth 2006; Brand et al. 2009; van Otterloo et al. 2013; Chako Tchambe et al. 2015). Experiments also showed that when explosions of a given energy occurred at deeper relative depths, and if a crater was already present above the explosion site, the ability of ejecta to travel ballistically out of a crater was limited and extracrater deposition occurred predominantly by dilute density currents through the expulsion of fine-grained particles and gas from the explosion jet collapsing into the crater (Graettinger et al. 2015a). Conversely, very shallow experiments transported only a small volume of material ballistically as more of the explosion energy was lost to the atmosphere (Graettinger et al. 2014).

Application of these facies-based interpretations is dependent on the discrimination of massive tuff breccias and lapilli tuffs from coarse-tail graded tuff breccias (Table 2). TBm shares several gross similarities with TBg, but they represent very different mechanisms of transport, deposition, and eruption conditions. The most distinctive characteristics of TBm include basal loading structures, massive structure in proximal and distal extent, mantling of topography, and jigsaw clasts, all of which reflect a hybrid between individual ballistic clast deposition and that of a mass of sliding debris. TBg, in contrast, is characterized by reverse to normal coarse-tail grading of blocks, gas escape structures, erosive basal contacts, and infill of topographic lows that reflect lateral transport in a concentrated dispersion. Additionally, coarse-tail graded tuff breccia is matrix-supported for its full extent, while the massive tuff breccia can vary between matrix- and clast-supported even at large distances. The blocks in both sequences are prominent, but TBg lacks the exceptionally large sedimentary lithic clasts and jigsaw clasts that occur in TBm (Fig. 9 versus Fig. 6a, b). Furthermore, TBm blocks show a wide range of shapes including very elongate shapes, while TBg contains more equant subrounded clasts. In addition to facies-specific characteristics, the associations of coarse-tail graded tuff breccia with fine bedded tuff (ATs) and massive tuff breccia with cross-bedded tuff (ATx) aide in the recognition of the two facies (Figs. 2 and 3). In the proximal region, some of these important diagnostic characteristics may be absent or obscured by erosion and deformation by ballistics. However, the presence of multiple couplets of TBm and ATx may be a fingerprint of the presence of deposits transported by ballistic curtains resulting from repeated discrete explosions through a debris-filled vent. Similar couplets at Haskie tuff ring, adjacent to Triplets, have been interpreted as the result of density stratification of a PDC with distance (Vazquez and Ort 2006), but the absence of flow indicators and abundance of loading structures in the TBm deposits in this study, and those described in Vazquez and Ort (2006), support a ballistic interpretation for the couplets at all three HBVF tephra rings. The interpretation of individual couplets requires detailed attention to the proximal to distal variation in a deposit (Sohn and Chough 1989) and the contact between the coarse-grained and finer-grained deposits. Furthermore, the formation and preservation of some of these characteristics are dependent on the grain size of the material that is ejected. Deposits lacking significant fine-grained material (i.e., Dry Lake maar, San Francisco Volcanic Field) may still contain couplets of coarse and finer pyroclastic units but lack the abundant ash-sized particles to produce the poor sorting or cross-beds observed in the HBVF. In such cases, however, other depositional characteristics may still preserve evidence of ballistic transport

Table 2 Comparison of deposits interpreted to form from ballistic curtains, concentrated PDCs, and dilute PDCs

	Ballistic curtain deposit	Concentrated PDC	Dilute PDC
Sorting	Poor	Poor	Moderate
Maximum grain size	Blocks proximal and distal	Blocks proximal and decreases with distance	Sand to lapilli
Basal contact	Undulatory, loading structures common	Erosional to conformable	Conformable
Matrix- versus clast-supported	Clast or matrix support	Matrix support	Matrix support
Percent contribution blocks	80%	40%	< 1%
Topography relationship	Mantles topography	Erodes proximal topography and distally fills topography	Drapes topography
Lateral thickness variations	Constructional proximal, sheet-like medial that thins progressively, and isolated clasts distal	Thins progressively with distance	Thins progressively with distance
Grading	None	Reverse to normal coarse-tail grading with highest concentration just above base	None
Componentry	Heterolithic and highly variable with distance and between beds	Heterolithic but fairly consistent with distance for a single bed	Heterolithic
Other features	Jigsaw fit clasts	Fines-depleted pipes	Cross-bedding

(sags) in the lower bed and lateral transport (piling up lapilli on the up-slope, ventward side of blocks) in the upper bed of couplets (Valentine 2012).

The identification of these field relationships can also be impeded by modification of deposits by subsequent events including erosion, formation of soft sediment deformation structures, water and wind reworking, and slumping proximal to the crater. Examples like the Udo Tuff Cone (Sohn and Chough 1993) and Dry Lake Maar (Valentine 2012) where ejecta were emplaced on steep slopes may have additional overprinting such as prolonged grain flow following primary ballistic emplacement or the impact of isolated ballistics on unconsolidated deposits. Thin beds on any slope can be particularly difficult to identify in proximal areas as blocks and bombs, or masses of debris emplaced ballistically, form sags, or even cut through multiple layers before coming to rest, mixing the transected deposits. Clasts transported ballistically can also be emplaced simultaneously with PDC deposits and locally disrupt structures or produce an obstacle disrupting bedding and sedimentary structures (Fig. 6). Observations of the eruption of Ukinrek maar indicate multiple vents may be active simultaneously and/or different eruption processes can occur simultaneously (Self et al. 1980). Therefore, it is possible that ballistic curtains and PDCs could be emplaced simultaneously, so that not just single clasts but also large masses of poorly sorted material are deposited on top/through a still moving PDC resulting in highly complex depositional structures. Complex deposit structures resulting from multiple distinct eruption mechanisms depositing material simultaneously have been described elsewhere (e.g., Rothenberg cone, Houghton and Schmincke 1986; La Palma, White and Schmincke 1999).

Variations in relative explosion position and energy

The recent evolution of conceptual models of phreatomagmatic eruptions has highlighted important questions about how a typical eruption sequence might evolve, including how many explosions occur and where (Valentine et al. 2017). The abundance of TBm and ATx couplets in the tephra rings described here indicates that material transport outside the crater during these eruptions is accomplished predominantly by repeated discrete explosions. Previous models have relied on host rock lithics to determine the depth of explosions, but it is now clear that these explosions sample material that has been mixed within the vent during an eruption and reflect the cumulative explosion history rather than individual events (Lefebvre et al. 2013; Graettinger et al. 2015a, 2016; Sweeney and Valentine 2015). There is also ample evidence through stratigraphic relationships, ballistic orientations, and morphology that vent locations within a crater migrate both vertically and laterally throughout an eruption (Ort and Carrasco-Núñez 2009; van Otterloo et al. 2013; Jordan et al. 2013; Pedrazzi et al. 2014; Agustin-Flores et al. 2015; Kosik et al. 2016). Individual clasts in a tephra ring therefore do not help constrain the depth of the explosion that produced the beds in which the lithics are hosted.

What then can we infer about the relative explosion depth from tephra ring deposits? Phreatomagmatic explosions are discrete localized events that produce outward propagating shock waves that fragment intruding magma as well as surrounding rock and other debris (Zimanowski et al. 1997; Büttner and Zimanowski 1998; Büttner et al. 2005). When these explosions occur in a debris-filled vent, the relative depth of the explosion, most easily discussed as scaled depth, influences whether material is transported out of the vent or confined to the subsurface (Valentine et al. 2014). Scaled depth (SD) relates physical depth to the absolute energy of an explosion, where $SD = depth/energy^{1/3}$ (Goto et al. 2001; Sonder et al. 2015). Scaled depth can be divided into regimes where explosions are close to optimal (excavate the greatest volume of ejecta for a given energy) and those that are either shallower than, or deeper than, that optimal scaled depth (Graettinger et al. 2014). Experiments have constrained an optimal scaled depth for discrete explosions through debris to ~ 0.004 $m/J^{1/3}$ and the depth where explosions are confined, and no ejecta is produced, to 0.008 $m/J^{1/3}$ (Goto et al. 2001; Graettinger et al. 2014; Valentine et al. 2014; Sonder et al. 2015). Explosions above the confinement depth transport material out of the vent, but the scaled depth and overlying topography (e.g., craters produced by previous explosions) influence how much material makes it out of the vent and the how it is transported away from the vent (Graettinger et al. 2014, 2015a). Therefore, it should be possible to qualitatively estimate the scaled depth regimes of explosions from facies associations within a tephra ring stratigraphy.

The Teshim and Triplets tephra rings contain facies associations that reflect processes similar to those in experiments and enable the estimation of generalized trends in the scaled depth regime of explosions during an eruption based on those signatures. It is not expected that individual eruptions are produced by only one scaled depth of explosion, or that it should be possible to interpret every bed in a tephra ring as the product of a specific explosion. Rather, we propose that facies associations within bed sets can be used to better reconstruct the scaled depth regime of phases in an eruption sequence including information on relative depth of explosions during a phase and a minimum number of shallow ejecta producing explosions. It is also important to note the likelihood of a preservation bias for near-optimal scaled depth explosion deposits as they transport the greatest volume of material out of a crater for a given explosion energy (Valentine et al. 2014); thus, a predominance of deposits from near-optimal scaled depth explosions in a tephra ring does not mean that such explosions were the most common during the eruptive episode. Nevertheless, these estimates would benefit any future hazard assessment of

individual volcanoes and phreatomagmatic-dominated volcanoes in general.

Using the revised stratigraphic descriptions from Teshim and Triplets tephra rings in combination with experimental observations, we propose that the following facies relationships can be interpreted as the result of a scaled depth regime for a phase of an eruption. First, couplets of alternating TBm and ATx are interpreted as the product of repeated near-optimal scaled depth explosions. Second, bed sets dominated by repeating beds of dune from or cross-bedded tuffs (ATx) are interpreted as the result of deeper-than-optimal scaled depth explosions where the bulk of explosion jet returns to the crater and fine-grained material escapes the crater in the form of dilute density currents. Third, bed sets dominated by only massive tuff breccias (TBm) reflect shallower-than-optimal scaled depth explosion conditions (Table 4). Fourth, concentrated PDCs require a sustained supply of pyroclastic material, and thus, the presence of coarse-grained PDC deposits is interpreted as the result of a semicontinuous eruption columns produced by closely timed phreatomagmatic explosions. Fifth, spatter (Sp), well-sorted lapilli tuff (LTw), and lavas are interpreted as the result of magmatic activity driven by exsolving volatiles.

An extrapolation of this approach to previously published tephra ring studies can be accomplished through the identification of major facies from this study in published stratigraphic descriptions and columns. This comparison includes the recognition of facies bearing the major characteristics described above and, if possible, the relative abundance of beds containing those features within a stratigraphic sequence (Table 3). ATx facies, cross-bedded ash and lapilli tuffs, have been described at most tephra rings and were frequently discussed in detail making recognition of ATx in published stratigraphic columns straightforward. A few detailed descriptions of coarse-tail graded tuff breccias facilitated the recognition of TBg in the literature. While TBm had not been previously described as a specific facies, descriptions of block-rich massive tuff breccias with loading structures were common in the reevaluated stratigraphic columns (Wohletz and Sheridan 1983; Sohn and Chough 1989; Brand et al. 2009). Descriptions of individual ballistic clasts, notably those forming bomb sags, were frequently included along in published stratigraphic sections and accompanied by a description of the surrounding unit, frequently having characteristics of TBm facies. TBm facies were also identified in published stratigraphic sections from descriptions of couplets of massive

Table 3 Occurrence of facies in stratigraphic sequences from this study and the published literature

	TBg	ATx	TBm	LTw, ATs, Sp, or other juvenile units
Teshim HBVF	Few	Common	Common	Common (ATs, LTw)
Triplets HBVF	Multiple	Dominant	Common	Present (LTw, Sp)
Haskie HBVF (Vazquez and Ort 2006)	Present	Common	Common	Few (LTw)
Atexcac, Mexico (Carrasco-Núñez et al. 2007; Lopez-Rojas and Carrasco-Núñez 2015)	Not described	Common	Common (couplets)	Present (scoria)
Easy Chair, USA (Valentine and Cortés 2013)	Few	Common	Common (couplets)	Present (Sp)
Dry Lake Maar (Valentine 2012)	Present	Absent	Common	Present (scoria)
Fort Rock, USA (Brand and Clarke 2009)	Not described	Common	Common	Present (Sp)
La Brena- El Jaguey, Mexico (Aranda-Gomez et al. 1992)	Not described	Common	Common	Present (scoria)
Mt Gambier, Australia (Van Otterloo et al. 2013; Van Otterloo and Cas 2016)	Present	Present	Present (couplets)	Common (scoria)
Nabrona Pass, USA (Brand et al. 2009)	Present	Common	Common	Present (Lava)
Salt Lake Craters, USA (Fisher and Waters 1970)	Not described	Common	Not described	Not described
Stracciacapa, Italy (Valentine et al. 2015)	Not described	Common	Common (couplets)	Present (scoria)
Suona Crater, Japan (Geshi et al. 2011)	Present	Absent	Present	Not described
Suwolbong tuff ring (Sohn and Chough 1989)	Present	Present	Present	Present (scoria)
Tepexitl, Mexico (Austin-Erickson et al. 2011)	Not described	Common	Present	Not described
Tihany maars, Hungary (Nemeth et al. 2001)	Present	Common	Present	Present (scoria)
Tito, Argentina (Haller and Nemeth 2006)	Not described	Present	Present	Not described
Ubehebe, USA (Fisher and Waters 1970; Fierstein and Hildreth 2017)	Present	Common	Not described	Present (scoria, Sp)
Zuni Salt Lake, USA (Fisher and Waters 1970)	Not described	Present	Present (couplets)	Present (scoria)

The term 'present' is used to avoid frequency implications except when frequency was well constrained. Unless explicitly stated, the absence of features is noted as 'not described' as studies may not have provided sufficient data to rule out their presence and 'absent' when explicitly noted as such

Table 4 Proposed reinterpretation of tephra ring stratigraphic sections based on this study to include estimates of the contribution of different scaled depth phreatomagmatic explosions

Example (reference)	Important observations	Interpretation
Teshim (this study)	Dominated by massive tuff breccias alternating with cross-bedded tuffs with large blocks throughout. Sequence starts and ends with pyroclastic fall deposits. Minimum couplets—7	Abundant near-optimal scaled depth discrete explosions with multiple phases of more magmatic activity at least one more sustained eruption column
Triplets (this study)	Base of sequence is dominated by dilute density current deposits. Up sequence, large blocks and alternating massive tuff breccias become more abundant. Scoriacious fall and agglutinate dominates cap sequence. Minimum couplets—10	Deeper-than-optimal scaled depth discrete explosions with occasional sustained activity, followed by shallowing of explosions to near-optimal scaled depth, and ended with Strombolian activity
Haskie (Vazquez and Ort 2006)	Abundant couplets of massive tuff breccias alternating with cross-bedded tuffs, some concentrated density current deposits Minimum couplets—6	Abundant near-optimal scaled depth discrete explosions ended with Strombolian activity
Atexcac (Carrasco-Núñez et al. 2007; López-Rojas and Carrasco-Núñez 2015)	Dominated by massive tuff breccias alternating with cross-bedded tuffs suggestive of ballistic curtains deposits paired with dilute density current deposits Minimum couplets—8–19	Abundant near-optimal scaled depth discrete explosions
Easy Chair (Valentine and Cortés 2013)	Basal sequence dominated by agglomerate deposits. Upper deposits are predominantly massive tuff breccias suggesting ballistic curtain deposits and possibly some dense pyroclastic flow deposits	Abundant by near-optimal and shallower-than-optimal scaled depth discrete explosions
Fort Rock (Brand and Clarke 2009)	Upper sequence is dominated by massive tuff breccias alternating with cross-bedded tuffs. Minimum couplets—13	Transitional between deeper-than-optimal and near-optimal scaled depth discrete explosions
La Brena-El Jaguey (Aranda-Gomez et al. 1992)	Alternating beds of clast-supported massive tuff breccias with finer grained bedded units with dune forms and bomb sags. Occasional scoriaceous fall deposits Minimum couplets—~ 30	Near-optimal scaled depth discrete explosions with intermittent Strombolian activity
Mt Gambier (Van Otterloo et al. 2013; Van Otterloo and Cas 2016)	Cross-bedded tuffs common, couplets of massive tuff breccias with cross-bedded tuffs Minimum couplets—9	Deeper-than-optimal and near-optimal scaled depth discrete explosions with some sustained columns
Narbona Pass Maar (Brand et al. 2009)	Dominated by alternating sequences of ballistic and dilute density current deposits. May also include concentrated density current deposits Minimum couplets—~ 30	Near-optimal scaled depth explosions with occasional more sustained eruptive phases
Salt Lake Craters (Fisher and Waters 1970)	Dune forms and fine-grained deposits dominate	Deeper-than-optimal scaled depth discrete explosions
Straciacappa (Valentine et al. 2015b)	Alternating massive lapilli tuff with cross-bedded tuffs. Fine-grained block-bearing unit at end of sequence Minimum couplets—8	Near-optimal scaled depth discrete explosions with possible shallowing at end of sequence
Suona Crater (Geshi et al. 2011)	Poorly sorted block-rich layers. Some erosional contacts visible, but lowest layer massive tuff breccias mantles topography suggesting some ballistic deposits and some concentrated density current deposits.	Near-optimal to shallower-than-optimal scaled depth discrete explosions with a sustained phase that collapsed to form dense pyroclastic density currents
Suwolbong tuff ring (Sohn and Chough 1989)	Abundant stratified to cross-stratified tuffs that transition upward to alternating massive tuff breccias and tuffs, capped by stratified tuffs	Deeper-than-optimal scaled depth discrete explosions that shallow to near-optimal scaled depth explosions
Tepexitl (Austin-Erickson et al. 2011)	Abundant alternating massive tuff breccias alternating with cross-bedded tuffs that could be ballistic curtain deposits Minimum couplets—16	Near-optimal scaled depth discrete explosions early with a possible transition to shallower-than-optimal scaled depth explosions
Tihany maars (Nemeth et al. 2001)	Dune form beds dominate lower sequence with increasing occurrence of massive tuff breccias alternating with cross-bedded tuffs Minimum couplets—6	Deeper-than-optimal scaled depth discrete explosions shallowing to near-optimal scaled depth explosions
Tito Maar (Haller and Nemeth 2006)	Repeating ballistic curtain deposits with dilute density current deposits	Shallower-than-optimal and near-optimal scaled depth discrete explosions
Ubehebe (Fisher and Waters 1970; Fierstein and Hildreth 2017)	Dominated by dune forms and fine-grained deposits	Deeper-than-optimal scaled depth discrete explosions with some near-optimal scaled depth explosions from early vents
Zuni Salt Lake (Fisher and Waters 1970; Onken and Forman 2017)	Dominated by dune forms with occasional alternating massive tuff breccias	Deeper-than-optimal scaled depth discrete explosions with some near-optimal scaled depth explosions

block-rich units alternating with cross-bedded tuffs that lacked any characteristics linked with lateral transport such as filling topographic lows, or gas escape pipes.

The examples from the HBVF from this study, and neighboring Haskie Maar (Vazquez and Ort 2006), reflect diverse eruption sequences where near-optimal scaled blasts, as reflected by the abundance of ATx and TBm couplets, were common, occurring in all three sequences (Table 3). These couplets were sometimes preceded by multiple repeating ATx deposits (Triplets; Fig. 3) reflecting multiple deeper-than-optimal scaled explosions prior to the near-optimal explosions. Such a sequence suggests that explosion locations can migrate upward during an eruption sequence. The deposits of discrete explosions are also interbedded with those from magmatic explosions like LTw or Sp (Teshim and Triplets). These sequences suggest that deposits produced by magmatic processes can occur at any time during an eruption, rather than through a systematic depletion of available water (Houghton and Schmincke 1986; van Otterloo et al. 2013; Valentine et al. 2015).

Stratigraphic sections from other volcanic fields contain additional diversity in the sequence of lithofacies, but couples of TBm and ATx are abundant, suggesting that discrete explosions at near-optimal scaled depth conditions are common and commonly preserved. Of the 19 tephra rings evaluated (Table 4), only two examples were dominated by TBm deposits without ATx interbeds, suggesting an eruption of predominantly shallower-than-optimal scaled depth explosions (Lunar Crater and Tito Maar). Seventeen tephra rings had some evidence of near-optimal scaled depth blasts, and seven, including Triplets, showed evidence of an episode dominated by deeper-than-optimal scaled depth blasts in the form of repeating cross-bedded tuffs (Atx). Nine sequences had deposits with descriptions of coarse-tail graded tuff breccia (TBg), interpreted as the result of concentrated PDCs (Table 3). Fifteen of the stratigraphic sequences involved descriptions of magmatic fall, spatter, or flow. The bulk of the deposits in published columns was the product of mafic magmas with the exception of Tepexitl in Mexico that involved rhyolitic magma (Austin-Erickson et al. 2011). This tephra ring contains very similar facies to the mafic examples but lacks a clear juvenile fall, lava unit, and concentrated PDC deposits. This suggests that the rhyolitic maar was excavated mainly by discrete explosions, including near-optimal scaled depth blasts (Table 4).

The published stratigraphic sections (Table 3) suggest that ballistic curtains are common in tephra rings, and thus, ballistic curtain processes from discrete explosions are common in maar-forming eruptions. We do not suggest that all deposits previously interpreted as the result of concentrated PDCs were interpreted incorrectly, rather, while individual concentrated PDC deposits (TBg) are recognized within phreatomagmatic tephra sequences (Fig. 2), tuff breccias that are part of TBm and ATx couplets likely reflect ballistic emplacement of ejecta and related dilute density currents.

This collection of previously published tephra ring descriptions is not exhaustive of available stratigraphic studies; nevertheless, the similarity of tephra ring stratigraphic sections, including the common presence of deposits associated with ballistic curtains, suggests that near-optimal scaled explosions occur in many phreatomagmatic eruption sequences. Abundance of such deposits in the tephra rings, however, does not suggest dominance, as tephra rings only preserve material successfully ejected by explosions and therefore may preferentially preserve the depositions of near-optimal scaled depth explosions. Minimum estimates from published stratigraphic columns reflects that the studied tephra rings contain anywhere from 6 to 30 couplets of TBm and Atx reflecting a minimum number of near-optimal discrete phreatomagmatic explosions that produced extracrater ejecta (Table 4). The number of nonoptimal explosions is far more difficult to constrain as counting individual beds in sequences of repeated ATx or TBm bed sets is more difficult. Nevertheless, it is possible to say that phreatomagmatic-dominated eruptions frequently produce tephra rings from an eruption sequence of discrete phreatomagmatic explosions with occasional sustained eruption columns when explosions are closely spaced in time and related fall of suspended fine ash.

This variability in eruption sequences and the common occurrence of near-optimal scaled depth explosions suggest that previous models of progressively deepening explosion positions as controlled by water drawdown (Lorenz 1986) do not match observations of many maar-diatremes.

Table 5 Minimum and conservative maximum estimates of deposit and eruption parameters for Teshim and Triplets tephra rings

	Minimum	Maximum
Deposit density (kg/m^3)	1900	2500
Deposit extent (m)	450	1000
Bed thickness (m)	0.1	0.5
Crater radius[a] (m)	400	500
Ejection angle (°)	15	60
Velocity from block Teshim[b] (m/s)	80	120
Velocity from block Triplets[c] (m/s)	70	100
Erupted volume (m^3)	1.28×10^5	1.70×10^6
Erupted mass (kg)	2.43×10^8	4.25×10^9
Explosion energy (J)	5.96×10^{11}	3.06×10^{13}
Explosion depth (m; near-optimal scaled depth)	30	115

[a] Triplets crater is 800 m in diameter and Teshim has 1000 m crater

[b] 20 cm diameter basaltic block 450 m from crater rim, estimated density of 2500 kg/m^3

[c] 65 cm diameter sandstone block 450 m from crater rim, estimated density of 2500 kg/m^3

Table 6 Equations used to calculate deposit mass and explosion energy and depth

Volume[a]	Frustum of a cone ($R^2 + Rr + r^2$)	R = distance from center block r = crater diameter
Mass	Density × volume	Density for poorly clastic deposit
Energy	$E = 1/2mv^2$	m = mass of individual bed derived from volume v = initial velocity from Eject!
Depth	$D = \text{SD} \times E^{1/3}$	SD = near-optimal scaled depth (0.004 m/J$^{1/3}$)

[a] This simplified volume was used to include the material moved by the explosion that returned to the crater as well as the ejecta on the tephra ring. This also assumes that the deposit is radially symmetrical

Importantly, this suggests that our understanding of the hydrology of diatremes, namely how water gains access to the melt in, and around, a diatreme to produce the conditions favorable for phreatomagmatic explosions, is sorely lacking. Further investigation of tephra rings focusing on signatures of minimum shallow explosion number, explosion depth, and relative contribution of different explosion styles will help inform our understanding of what constitutes a typical maar eruption.

Quantifying explosion energy and depth

This analysis can be taken another step by leveraging the well-exposed ballistic curtain deposits from the HBVF as representatives of near-optimal scaled depth explosion deposits. The largest ballistic blocks found at a distance of 450 m within the typical example of TBm deposits in Teshim and Triplets were measured (0.2 m ballistic block Teshim and 0.65 m sandstone block Triplets). The program Eject! (Mastin 2001) was then used to calculate initial velocities for these blocks over a range of ejection angles assuming ejection from the center of the crater and zero drag. Block ejection velocity increases for very low and very steep angles and did not exceed 120 m/s for either block, with minimum velocities of 70–80 m/s at 45°. These values were then used as the minimum and maximum likely ejection velocities for the deposits containing the blocks (Table 5). Volume estimates for individual beds are based on proximal thickness and distal extent. A range of volumes is calculated with a minimum volume using the distance the block traveled (0.45 km) as the deposit extent and a conservative maximum based on the observed extent of the tephra ring (1 km). These estimates use bed thicknesses of 0.1–0.5 m to represent the range of individual bed volumes present in the two tephra rings (Table 6). Mass is calculated from this volume using an estimated density of 1900–2500 kg/m^3 for the poorly sorted clastic deposit (Table 6). The kinetic energy (KE) required to move the mass of material at the initial ejection velocity can then be estimated using $\text{KE} = 1/2mv^2$ (Table 5-6), m being mass and v being velocity. If these explosions occurred at an optimal scaled depth of 0.004 m/J$^{1/3}$, they would have occurred at depths of 10–115 m (Tables 5 and 6). The estimated explosion energies of 10^{11}–10^{13} J and the depth for optimal scaled depth explosions from HBVF fit well

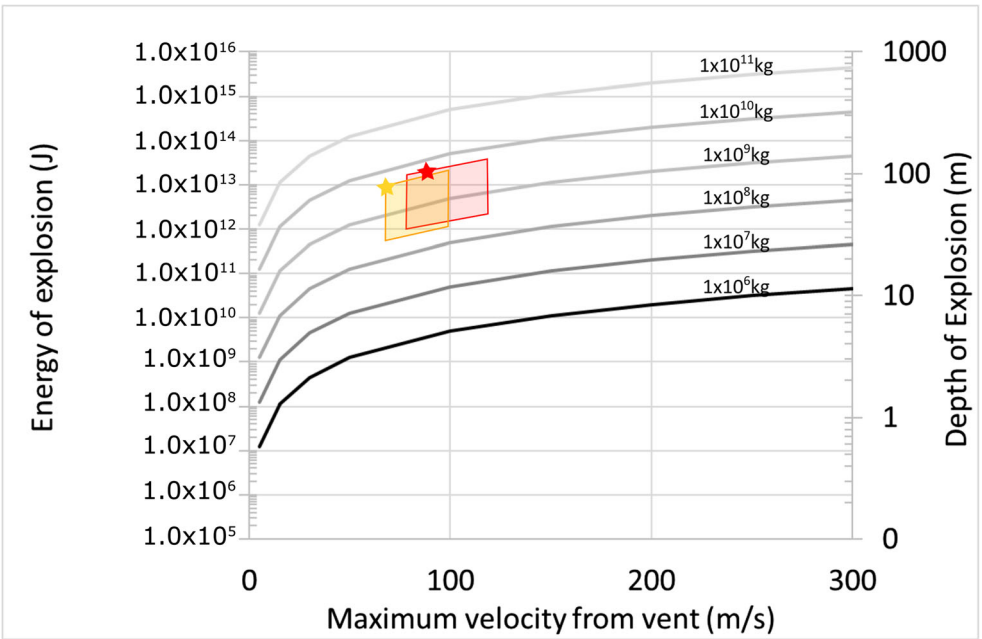

Fig. 11 Plot of explosion energy, ejection velocity, and physical depth of explosion for near-optimal scaled depth explosions for a range of ejected masses (gray lines) constrained with HBVF observations and estimates from Valentine et al. (2014). Colored boxes reflect minimums and conservative maximum estimates for Teshim (red) and Triplets (yellow) deposits (see Table 4). The stars represent estimates for a maximum deposit volume at 45° ejection angle for the respective tephra rings

within the range of phreatomagmatic explosion energies calculated from intrusion volumes and phreatomagmatic explosion efficiency by Valentine et al. (2014). After establishing estimates based on natural deposits, this process is extended to hypothetical deposit masses (10^6–10^{11} kg) and an expanded range of initial velocities (0–300 m/s; Fig. 11). For ejection velocities ≤ 100 m/s, the estimated explosion energies ranged from 10^9 to 10^{14} J with depths 10–500 m. This supports the estimates of Valentine et al. (2014) that most discrete phreatomagmatic explosions that contribute to tephra rings are likely 10^9–10^{12} J and occur at depths of < 250 m (Fig. 11). As expected, the energy increases with deposit mass, but the calculations are sensitive to low ejection velocities (0–50 m/s). This means the ability to calculate an explosion energy is dependent on the presence of ballistics large enough to reconstruct velocity and may underestimate energy for a deposit that has a limited coarse fraction due to the lack of available clast sizes, rather than being velocity limited. This approach could be easily applied to other phreatomagmatic deposits to further constrain the range of explosion energies and explosion depths for optimal scaled depth explosions that produce large volumes of ejecta.

Conclusions

This detailed investigation of tephra rings with a revised focus on facies and facies relationships rather than just grain size variations enabled the recognition of distinct depositional facies that reflect the major modes of transportation and deposition of ejecta during phreatomagmatic-dominated eruptions. The depositional signatures of ballistic curtain transport and dilute density currents produced by discrete explosions through a debris-filled vent, sustained activity that fed pyroclastic density currents, and delayed fall of suspended clasts were recognized through field observations and resulted in reevaluation of published tephra ring stratigraphic sections. Variable proportions of these deposits representing different transports and depositional processes are documented within a single volcanic field (this study; Vazquez and Ort 2006) and across previously published observations from 15 volcanic fields (Table 4). The variability is interpreted as the result of migrating phreatomagmatic explosion locations vertically and laterally, variations in the timing of explosions (discrete versus multiple and closely spaced in time), and temporary and permanent transitions to magmatic explosion mechanisms. The signatures of varying efficiencies of magma water interactions are likely still present in these deposits, but they are overprinted by those processes that occur after the explosion, namely transport and deposition. It is also necessary to recognize that tephra rings only contain material that was successfully ejected from the crater, and likely preferentially preserves deposits from near-optimal scaled explosions.

The comparison of multiple tephra rings is important for constraining what is common across maar-forming eruptions. The occurrence of couplets of tuff breccias and lapilli tuffs with stratified to cross-bedded ash and lapilli tuff deposits is common among the tephra rings in the literature discussed, suggesting that near-optimal scaled depth discrete explosions are common in phreatomagmatic-dominated eruptions. Further, the deposits were used to estimate explosion energies and ejection velocities responsible for beds within these tephra rings produced by near-optimal scaled depth explosions (> 10^{11} J, < 100 m/s). As near-optimal scaled depth explosions effectively transport large volumes of material and large blocks, the ability to relate deposit signatures to eruptive processes is necessary to anticipate future hazards from phreatomagmatic eruptions. The deposits of concentrated pyroclastic density currents, reflecting sustained activity relative to individual phreatomagmatic explosions, and the deposits of magmatic volatile-driven activity occur at any time within these depositional sequences and suggest that these eruptions are highly variable and do not follow simple progressions related to the consumption of available water.

Acknowledgments Karoly Nemeth and an anonymous reviewer are thanked for their comments. Thanks to Michael Ort for useful discussions and suggesting the inclusion of the Triplets in this work. Thanks are also extended to James White for feedback and discussion on an early version of this manuscript. Janine Krippner and Robin Wham are thanked for their field assistance. Field work was conducted on the Navajo Nation under a permit from the Navajo Nation Minerals Department, and any persons wishing to conduct geologic investigations on the Navajo Nation must first apply for and receive a permit from the Navajo Nations Minerals Department, P.O. Box 1910, Window Rock, Arizona 865115. A course module by the authors, and based on the work presented here, on maar-diatremes with two 50-min lectures and exercises is available https://vhub.org/resources/4045.

Funding information This work was funded in part by the National Science Foundation EAGER and 3E fund from the University at Buffalo.

References

Agustin-Flores J, Nemeth K, Cronin SJ, Lindsay JM, Kereszturi G (2015) Construction of the North Head (Maungauika) tuff cone: a product of Surtseyan volcanism, rare in the Auckland Volcanic Field, New Zealand. Bull Volcanol 77(2). https://doi.org/10.1007/s00445-014-0892-9

Aranda-Gomez JJ, Luhr JF, Pier JG (1992) The La Brena-El Jaguey Maar Complex, Durango, Mexico: I. Geological evolution. Bull Volcanol 54(5):393–404. https://doi.org/10.1007/BF00312321

Austin-Erickson A, Ort M, Carrasco-Núñez G (2011) Rhyolitic phreatomagmatism explored: Tepexitl tuff ring (Eastern Mexican

Volcanic Belt). J Volcanol Geotherm Res 201(1-4):325–341. https://doi.org/10.1016/j.jvolgeores.2010.09.007

Belousov A, Voight B, Belousova M (2007) Directed blasts and blast-generated pyroclastic density currents: a comparison of the Bezymianny 1956, Mount St. Helens 1980, and Soufriere Hills, Montserrat 1997 eruptions and deposits. Bull Volcanol 69(7):701–740. https://doi.org/10.1007/s00445-006-0109-y

Brand BD, Clarke AB (2009) The architecture, eruptive history, and evolution of the Table Rock Complex, Oregon: from a Surtseyan to an energetic maar eruption. J Volcanol Geotherm Res 180(2-4): 203–224. https://doi.org/10.1016/j.jvolgeores.2008.10.011

Brand BD, Clarke AB, Semken S (2009) Eruptive conditions and depositional processes of Narbona Pass Maar volcano, Navajo volcanic field, Navajo Nation, New Mexico (USA). Bull Volcanol 71(1):49–77. https://doi.org/10.1007/s00445-008-0209-y

Breard ECP, Lube G, Cronin SJ, Valentine GA (2015) Transport and deposition processes of the hydrothermal blast of the 6 August 2012 Te Maari eruption, Mt. Tongariro. Bull Volcanol 77(11). https://doi.org/10.1007/s00445-015-0980-5

Büttner R, Zimanowski B (1998) Physics of thermohydraulic explosions. Phys Rev 57:5726–5730

Büttner R, Zimanowski B, Mohrholz CO, Kummel R (2005) Analysis of thermohydraulic explosion energetics. J Appl Phys 98(4):043524. https://doi.org/10.1063/1.2033149

Carrasco-Núñez G, Ort MH, Romero C (2007) Evolution and hydrological conditions of a maar volcano (Atexcac crater, eastern Mexico). J Volcanol Geotherm Res 159(1-3):179–197. https://doi.org/10.1016/j.jvolgeores.2006.07.001

Chako Tchambe B, Ohba T, Kereszturi G, Nemeth K, Aka FT, Youmen D, Issa, Miyabuchi Y, Ooki S, Tanyileke G, Hell JV (2015) Towards the reconstruction of the shallow plumbing system of the Barombi Mbo Maar (Cameroon)—implications for diatreme growth processes of a polygenetic maar volcano. J Volcanol Geotherm Res 301: 293–313. https://doi.org/10.1016/j.jvolgeores.2015.06.004

Fierstein J, Hildreth W (2017) Eruptive history of the Ubehebe Crater cluster, Death Valley, California. J Volcanol Geotherm Res 335: 128–146. https://doi.org/10.1016/j.jvolgeores.2017.02.010

Fisher RV, Waters AC (1970) Base surge bed forms in maar volcanoes. Am J Sci 268(2):157–180. https://doi.org/10.2475/ajs.268.2.157

Fisher RV, Schmincke HU (1984) Pyroclastic rocks. Springer, Berlin, p 472

Geshi N, Németh K, Oikawa T (2011) Growth of phreatomagmatic explosion craters: a model inferred from Suoana crater in Miyakejima Volcano, Japan. J Volcanol Geotherm Res 201(1–4):30–38. https://doi.org/10.1016/j.jvolgeores.2010.11.012

Goto A, Taniguchi H, Yoshida M, Ohba T, Oshima H (2001) Effects of explosion energy and depth to the formation of blast wave and crater: field explosion experiment for the understanding of volcanic explosion. Geophys Res Lett 28(22):4287–4290. https://doi.org/10.1029/2001GL013213

Graettinger AH, Valentine GA, Sonder I (2016) Recycling in debris-filled volcanic vents. Geology 44(10):811–814. https://doi.org/10.1130/G38081.1

Graettinger AH, Valentine GA, Sonder I, Ross P-S, White JDL, Taddeucci J (2014) Maar-diatreme geometry and deposits: subsurface blast experiments with variable explosion depth. Geochem Geophys Geosyst 15(3):740–764. https://doi.org/10.1002/2013GC005198

Graettinger AH, Valentine GA, Sonder I, Ross PS, White JDL (2015a) Facies distribution of ejecta in analog tephra rings from experiments with single and multiple subsurface explosions. Bull Volcanol 77(8): 66. https://doi.org/10.1007/s00445-015-0951-x

Graettinger AH, Valentine GA, Sonder I (2015b) Circum-crater variability of deposits from discrete, laterally and vertically migrating volcanic explosions: experimental evidence and field implications. J Volcanol Geotherm Res 308:61–69. https://doi.org/10.1016/j.jvolgeores.2015.10.019

Haller MJ, Nemeth K (2006) Architecture and pyroclastic succession of a small Quaternary (?) maar in the Pali Aike Volcanic Field, Santa Cruz, Argentina. Zeitschrift der Deutschen Gesellschaft fur Geowissenschaften 157(3):155–164. https://doi.org/10.1127/1860-1804/2006/0157-0155

Houghton BF, Schmincke H-U (1986) Mixed deposits of simultaneous strombolian and phreatomagmatic volcanism: Rothenberg Volcano, East Eifel Volcanic Field. J Volcanol Geotherm Res 30(1–2):117–130. https://doi.org/10.1016/0377-0273(86)90069-7

Jordan SC, Cas RAF, Hayman PC (2013) The origin of a large (>3 km) maar volcano by coalescence of multiple shallow craters: Lake Purrumbete maar, southeastern Australia. J Volcanol Geotherm Res 254:5–22. https://doi.org/10.1016/j.jvolgeores.2012.12.019

Kosik S, Nemeth K, Kereszturi G, Procter JN, Zellmer GF, Geshi N (2016) Phreatomagmatic and water-influenced Strombolian eruptions of a small-volume parasitic cone complex on the southern ringplain of Mt. Ruapehu, New Zealand: facies architecture and eruption mechanisms of the Ohakune Volcanic Complex controlled by an unstable fissure eruption. J Volcanol Geotherm Res. https://doi.org/10.1016/j.jvolgeores.2016.07.005

Lefebvre NS, White JDL, Kjarsgaard BA (2013) Unbedded diatreme deposits reveal maar-diatreme forming eruptive processes: Standing Rocks West, Hopi Buttes, Navajo Nation, USA. Bull Volcanol 75(8):739. https://doi.org/10.1007/s00445-013-0739-9

López-Rojas M, Carrasco-Núñez G (2015) Depositional facies and migration of the eruptive loci for Atexcac axalapazco (central Mexico): implications for the morphology of the crater. Revista Mexicana de Ciencias Geologicas 32(3):377–394

Lorenz V (1986) On the growth of maars and diatremes and its relevance to the formation of tuff rings. Bull Volcanol 48(5):265–274. https://doi.org/10.1007/BF01081755

Mastin LG (2001) A simple calculator of ballistic trajectories for blocks ejected during volcanic eruptions: U.S. Geological Survey Open-File Report 01-45:https://pubs.usgs.gov/of/2001/0045/

Moore JG (1967) Base surge in recent volcanic eruptions. Bull Volcanol 30(1):337–363. https://doi.org/10.1007/BF02597678

Muirhead JD, Van Eaton AR, Re G, White JDL, Ort M (2016) Monogenetic volcanoes fed by interconnected dikes and sills in the Hopi Buttes volcanic field, Navajo Nation, USA. Bull Volcanol 78(11). https://doi.org/10.1007/s00445-016-1005-8

Nemeth K, Martin U, Harangi S (2001) Miocene phreatomagmatic volcanism at Tihany (Pannonian Basin, Hungary). J Volcanol Geotherm Res 111(1-4):111–135. https://doi.org/10.1016/S0377-0273(01)00223-2

Nemeth K, Cronin SJ, Smith IEM, Agustin-Flores J (2012) Amplified hazard of small-volume monogenetic eruptions due to environmental controls, Orakei Basin, Auckland Volcanic Field, New Zealand. Bull Volcanol 74(9):2121–2137. https://doi.org/10.1007/s00445-012-0653-6

Newkirk T (2009) Anisotropy of magnetic susceptibility of phreatomagmatic surge deposits, Hopi Buttes, Navajo Nation, Arizona, USA. In: Geology. Northern Arizona University, p 97

Onken J, Forman S (2017) Terminal Pleistocene to early Holocene volcanic eruptions at Zuni Salt Lake, west-central New Mexico, USA. Bull Volcanol 79:10. https://doi.org/10.1007/s00445-016-1089-1

Ort MH, Carrasco-Núñez G (2009) Lateral vent migration during phreatomagmatic and magmatic eruptions at Tecuitlapa Maar, east-central Mexico. J Volcanol Geotherm Res 181(1-2):67–77. https://doi.org/10.1016/j.jvolgeores.2009.01.003

Pedrazzi D, Aguirre Diaz G, Bartolini S, Marti J, Geyer A (2014) The 1970 eruption on Deception Island (Antarctica): eruptive dynamics and implications for volcanic hazards. J Geol Soc Lond 171(6):765–778. https://doi.org/10.1144/jgs2014-015

Self S, Kienle J, Huot J-P (1980) Ukinrek Maars, Alaska, II. Deposits and formations of the 1977 craters. J Volcanol Geotherm Res 7(1–2):39–65. https://doi.org/10.1016/0377-0273(80)90019-0

Sonder I, Graettinger AH, Valentine GA (2015) Scaling multiblast craters: general approach and application to volcanic craters. J Geophys Res 120(9):6141–6158. https://doi.org/10.1002/2015JB012018

Sohn YK, Chough SK (1993) The Udo tuff cone, Cheju Island, South Korea: transformation of pyroclastic fall into debris fall and grain flow on a steep volcanic cone slope. Sedimentology 40:769–786

Sohn YK, Chough SK (1989) Depositional processes of the Suwolbon tuff ring, Cheju Island (Korea). Sedimentology 36(5):837–856. https://doi.org/10.1111/j.1365-3091.1989.tb01749.x

Sweeney MR, Valentine GA (2015) Transport and mixing dynamics from explosions in debris-filled volcanic conduits: numerical results and implications for maar-diatreme volcanoes. Earth Planet Sci Lett 425:64–76. https://doi.org/10.1016/j.epsl.2015.05.038

Taddeucci J, Valentine GA, Sonder I, White JDL, Ross P-S, Scarlato P (2013) The effect of pre-existing crater on the initial development of explosive volcanic eruptions: an experimental investigation. Geophys Res Lett 40(3):507–510. https://doi.org/10.1002/grl.50176

Valentine GA (2012) Shallow plumbing systems for small-volume basaltic volcanoes, 2: evidence from crustal xenoliths at scoria cones and maars. J Volcanol Geotherm Res 223–224:47–63. https://doi.org/10.1016/j.jvolgeores.2012.01.012

Valentine GA, Cortés JA (2013) Time and space variations in magmatic and phreatomagmatic eruptive processes at Easy Chair (Lunar Crater Volcanic Field, Nevada, USA). Bull Volcanol 75(9):752–765. https://doi.org/10.1007/s00445-013-0752-z

Valentine GA, Graettinger AH, Sonder I (2014) Explosion depths for phreatomagmatic eruptions. Geophys Res Lett 41(9):3045–3051. https://doi.org/10.1002/2014GL060096

Valentine GA, Sottili G, Palladino DM, Taddeucci J (2015) Tephra ring interpretation in light of evolving maar-diatreme concepts: Stracciacappa maar (central Italy). J Volcanol Geotherm Res 308:19–29. https://doi.org/10.1016/j.jvolgeores.2015.10.010

Valentine GA, White JDL, Ross P-S, Graettinger AH, Sonder I (2017) Updates to concepts on phreatomagmatic maar-diatremes and their pyroclastic deposits. Front Earth Sci 5. https://doi.org/10.3389/feart.2017.00068

van Otterloo J, Cas RAF, Sheard MJ (2013) Eruption processes and deposit characteristics at the monogenetic Mt. Gambier Volcanic Complex, SE Australia: implications for alternating magmatic and phreatomagmatic activity. Bull Volcanol 75(8):737. https://doi.org/10.1007/s00445-013-0737-y

van Otterloo J, Cas RAF (2016) Low-temperature emplacement of phreatomagmatic pyroclastic flow deposits at the monogenetic Mt Gambier Volcanic Complex, South Australia, and their relevance for understanding some deposits in diatremes. J Geol Soc 173(4):701–710. https://doi.org/10.1144/jgs2015-122

Vazquez JA, Ort MH (2006) Facies variation of eruption units produced by the passage of single pyroclastic surge currents, Hopi Buttes volcanic field, USA. J Volcanol Geotherm Res 154(3-4):222–236. https://doi.org/10.1016/j.jvolgeores.2006.01.003

Waters AC, Fisher RV (1971) Base surges and their deposits: Capelinhos and Taal Volcanoes. J Geophys Res 76(23):5596–5614. https://doi.org/10.1029/JB076i023p05596

White JDL (1991) Maar-diatreme phreatomagmatism at Hopi Buttes, Navajo Nation (Arizona), USA. Bull Volcanol 53(4):239–258. https://doi.org/10.1007/BF00414522

White JDL, Schmincke H-U (1999) Phreatomagmatic eruptive and depositional processes during the 1949 eruption on La Palma (Canary Islands). J Volcanol Geotherm Res 94(1-4):283–304. https://doi.org/10.1016/S0377-0273(99)00108-0

White JDL, Valentine GA (2016) Magmatic versus phreatomagmatic fragmentation: absence of evidence is not evidence of absence. Geosphere 12(5):1478–1488. https://doi.org/10.1130/GES01337.1

Wohletz K, Sheridan MF (1983) Hydrovolcanic explosions II. Evolution of basaltic tuff rings and tuff cones. Am J Sci 283(5):385–413. https://doi.org/10.2475/ajs.283.5.385

Zimanowski B, Büttner R, Lorenz V (1997) Premixing of magma and water in MFCI experiments. Bull Volcanol 58(6):491–495. https://doi.org/10.1007/s004450050157